Title
Natural killer cells activated through NKG2D mediate lung ischemia-reperfusion injury.

Journal
The Journal of clinical investigation, 131(3)

ISSN
0021-9738

Authors
Calabrese, Daniel R
Aminian, Emily
Mallavia, Benat
et al.

Publication Date
2021-02-01

DOI
10.1172/jci137047

Peer reviewed

JCI The Journal of Clinical Investigation

Natural killer cells activated through NKG2D mediate lung ischemia-reperfusion injury

Daniel R. Calabrese, … , Mark R. Looney, John R. Greenland

J Clin Invest. 2020. https://doi.org/10.1172/JCI137047.

Research In-Press Preview **Immunology** **Pulmonology**

Graphical abstract

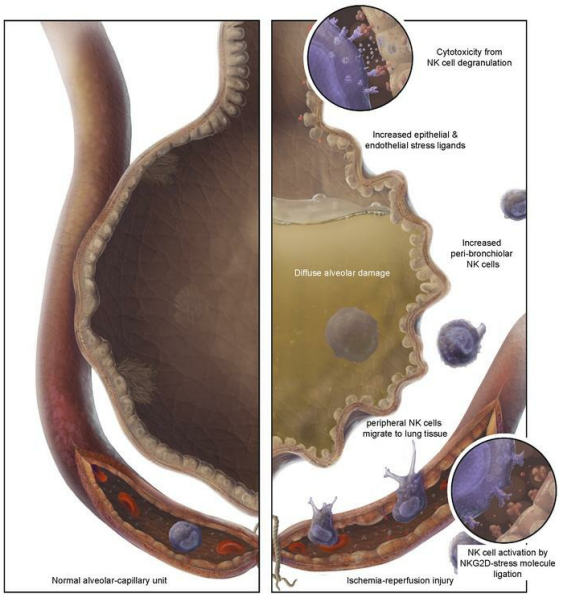

Natural killer cells activated through NKG2D mediate lung ischemia-reperfusion injury

Authors: Daniel R. Calabrese[1,2,*], Emily Aminian[1], Benat Mallavia[1], Fengchun Liu[1], Simon J.Cleary[1], Oscar A. Aguilar[3], Ping Wang[1], Jonathan P. Singer[1], Steven R. Hays[1], Jeffrey A. Golden[1], Jasleen Kukreja[4], Daniel Dugger[2], Mary Nakamura[1,2], Lewis L. Lanier[3], Mark R. Looney[1], John R. Greenland[1,2]

Affiliations:
[1]Department of Medicine, University of California, San Francisco, CA
[2]Medical Service, Veterans Affairs Health Care System, San Francisco, CA.
[3]Department of Microbiology and Immunology, University of California, San Francisco, CA and the Parker Institute for Cancer Immunotherapy San Francisco, CA
[4]Department of Surgery, University of California, San Francisco, CA
**Corresponding author*

Correspondence and reprint requests:
Dr. Daniel R. Calabrese,
San Francisco VA Medical Center,
4150 Clement St
San Francisco, CA 94121, USA
415-221-4810
daniel.calabrese@ucsf.edu

Graphical abstract

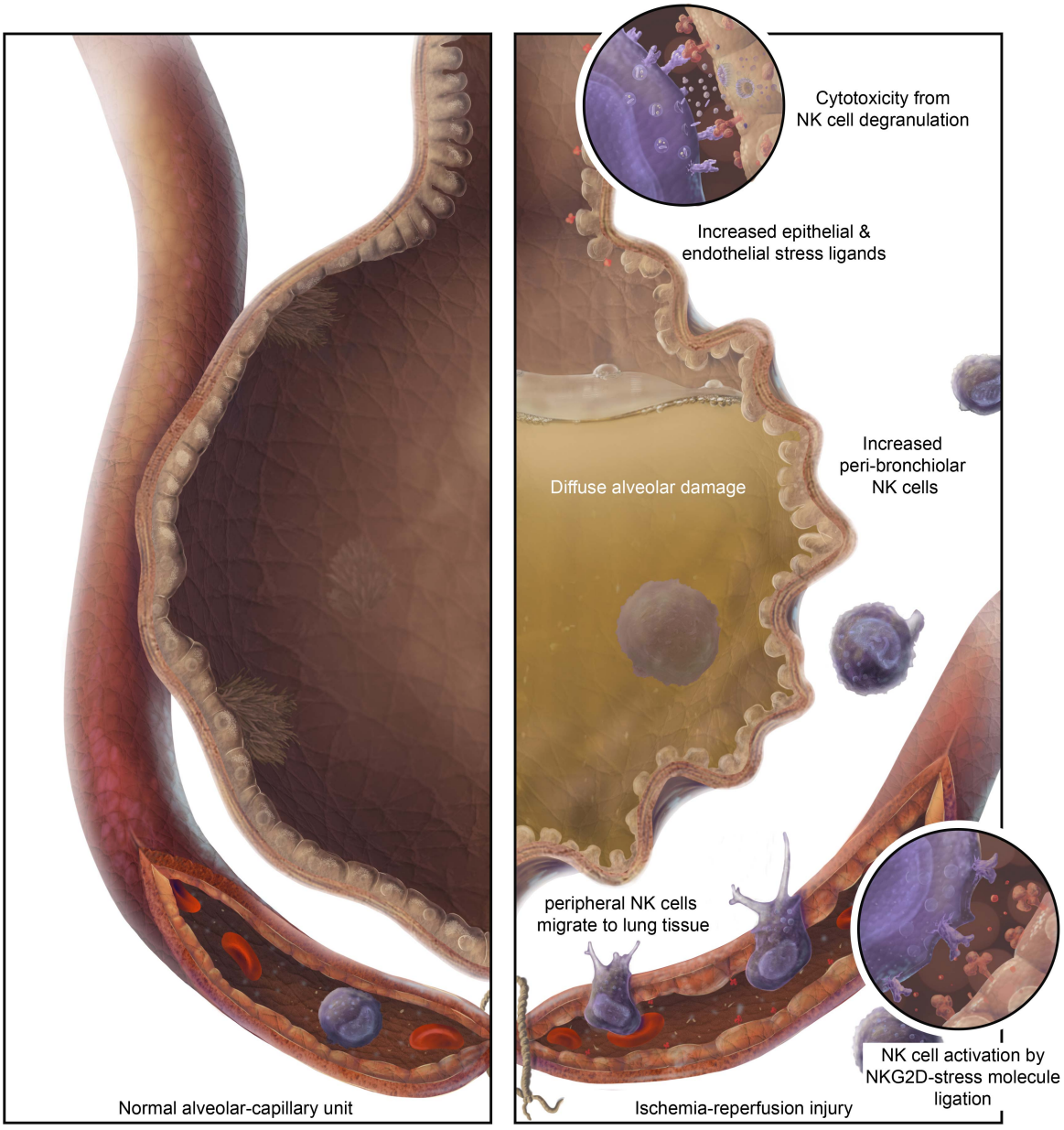

Abstract

Pulmonary ischemia-reperfusion injury (IRI) is a clinical syndrome of acute lung injury that occurs after lung transplantation or remote organ ischemia. IRI causes early mortality and has no effective therapies. While natural killer (NK) cells are innate lymphocytes capable of recognizing injured cells, their roles in acute lung injury are incompletely understood. Here, we demonstrated that NK cells were increased in frequency and cytotoxicity in two different IRI mouse models. We showed that NK cells trafficked to the lung tissue from peripheral reservoirs and were more mature within lung tissue. Acute lung ischemia-reperfusion injury was blunted in a NK cell-deficient mouse strain but restored with adoptive transfer of NK cells. Mechanistically, NK cell NKG2D receptor ligands were induced on lung endothelial and epithelial cells following IRI, and antibody-mediated NK cell depletion or NKG2D stress receptor blockade abrogated acute lung injury. In human lung tissue, NK cells were increased at sites of ischemia-reperfusion injury and activated NK cells were increased in prospectively collected human bronchoalveolar lavage in subjects with severe IRI. These data support a causal role for recipient peripheral NK cells in pulmonary IRI via NK cell NKG2D receptor ligation. Therapies targeting NK cells may hold promise in acute lung injury.

Introduction

Pulmonary ischemia-reperfusion injury (IRI) is a severe complication following lung transplant that causes primary graft dysfunction (PGD) within 72 hours in 1/3 of all lung transplant surgeries. Lung transplant is a potentially life-prolonging therapy for patients with end-stage lung disease, however, potential benefits are limited due to complications which cause some of the highest rates of morbidity and mortality among any solid organ transplant group (1). Early severe ischemia-reperfusion injury, manifesting clinically as primary graft dysfunction (PGD), is a major risk factor for chronic lung allograft dysfunction (CLAD) (2). PGD has no effective therapies and also accounts for nearly 50% of the mortality observed within the first year after lung transplantation (3, 4).

PGD shares clinical features with acute respiratory distress syndrome (ARDS) and is distinct from acute rejection (5, 6). Similar to ARDS, it is marked by alveolar-capillary barrier disruption and is diagnosed by bilateral pulmonary opacities and a ratio of arterial oxygen pressure to inspired oxygen content (PaO2/FiO2) less than 300 (3, 4, 7). However, distinct from other causes of ARDS, the inflammatory cascade from ischemia-reperfusion injury (IRI) is thought to play a central pathophysiologic role in PGD (8, 9).

Natural killer (NK) cells are innate immune cells that constitute up to 15% of resident lung lymphocytes (10). NK cells can be activated by the recognition of epithelial and endothelial stress molecules (11). Ischemia-reperfusion injury leads to HIF-1α upregulation and induction of these surface cellular stress molecules (12). Upon binding to the NK cell NKG2D receptor, damage signals initiate cytotoxic responses, particularly in mature NK cells (13-16). Outside of the lung, there is evidence that NK cells are important to other ischemia-reperfusion injury responses, such as ischemic cerebrovascular and renal disease, through several mechanisms (13-17).

While other innate immune cells including macrophages and neutrophils have been suggested to play a role in the acute lung injury of PGD, the role of NK cells has been incompletely explored.

Here, we tested the hypothesis that NK cells mediate pulmonary IRI through recognition of stress ligands in tissue that has been re-perfused following ischemia and hypoxia.

Results

NK cells are increased in the hilar clamp experimental mouse model of pulmonary IRI

To test whether NK cells were increased during pulmonary IRI, C57BL/6 mice were subjected to either hilar clamp (HC) procedure or a sham procedure (Figure 1A). We found that the proportion of NK cells (CD3-NKp46+) was significantly increased in injured, HC lungs compared to uninjured, sham lungs (Figure 1B). Similarly, absolute numbers of NK cells were increased in acutely injured lungs (Figure 1C, $p = 0.04$). As several other immune cells are capable of similar functions, we also measured T cells expressing NKp46 (CD3+NKp46+), CD8+ T cells (CD3+CD8+), and myeloid cells (CD3-CD11b+NKp46-). NKp46+ T cells were rare but were increased in lungs subjected to hilar clamp by frequency (Figure 1D) and total cell count (Figure 1E). There were no differences in the frequency or count of CD8+ T cells (Figure 1F and 1G) or myeloid cells (Figure 1H and 1I) in hilar clamp lungs compared to sham lungs. These data suggest that NK cells are the primary early responders in this group of effector cells.

NK cells are more mature and cytotoxic during experimental IRI

With maturation, NK cells gain cytotoxic and effector functions (18). In the mouse, this maturation pattern is characterized by a loss of surface CD27 and gain of surface CD11b in a progression depicted in Figure 2A. To assess differences in NK cell maturation during IRI, we measured CD11b and CD27 surface markers in digested C57BL/6 mouse HC and sham lungs. We found no differences in immature NK cell frequencies between lungs subjected to HC or sham surgery (Figure 2B-D). However, we found increased frequencies of mature NK cells (CD27-CD11b+) in HC lungs (Figure 2E). Upon cytotoxic NK cell degranulation, lysosomal membrane protein CD107a is increased on the cell surface (Figure 2F) (19). We found increased CD107a+ NK cells

by percent (Figure 2G, p = 0.002) and by MFI on NK cells (Figure 1H, p = 0.07) from HC compared to sham lungs. NKG2D is an activating receptor that recognizes stress molecules and is expressed at steady state on most NK cells. Notably, we found over 95% of NK cells from both sham and hilar clamp lungs were positive for NKG2D (Figure 2I). However, there was an increased density by median fluorescent intensity of NKG2D on NK cells of lungs subjected to hilar clamp (Figure 2J, p = 0.005). Following IRI, NKG2D was not increased on other T cell subsets (Supplemental Figure 1). Independent of cytotoxicity, we speculated that IRI might be associated with increased NK cell intracellular IFNγ and TNFα secretion. However, we found no differences in either IFNγ or TNFα intracellular cytokine staining in unstimulated NK cells following IRI (Supplemental Figure 2).

Mice lacking NK cells have less acute lung injury

To test if the absence of lymphocytes resulted in reduced lung injury, we performed HC surgeries on immunodeficient *Il2rg*$^{-/-}$*Rag2*$^{-/-}$ C57BL/6 mice, which lack NK, T, and B cells. Measures of acute lung injury were compared against wildtype C57BL/6 mice undergoing HC or sham procedures (Figure 3A). Representative H&E histopathology preparations are displayed in Figure 3B and show diffuse alveolar damage (DAD) characterized by hyaline membrane formation, intra-alveolar edema, capillary congestion, and neutrophilic infiltration in wildtype lungs. In contrast, no acute histopathology was observed in sham lungs, and significantly attenuated injury was documented in *Il2rg*$^{-/-}$*Rag2*$^{-/-}$ lungs subjected to HC. Quantitative injury measurements agree with these findings. Compared to wildtype HC lungs, there was reduced lung edema by extravascular lung water volume (EVLW) in wildtype sham mice and immunodeficient mice (Figure 3C). Additionally, we measured lung vascular permeability after intravenous injection of ^{125}I radiolabeled albumin, and there were less gamma counts recorded per gram of dry lung weight in sham lungs and immunodeficient lungs (*Il2rg*$^{-/-}$*/Rag2*$^{-/-}$) compared to HC procedures in wildtype mice (Figure 3D) and less endothelial permeability (Figure 3E). These findings demonstrate that mice lacking NK

cells have significantly reduced injury compared to wildtype mice subjected to experimental ischemia-reperfusion injury.

NK cell adoptive transfer into immunodeficient mice restores acute lung injury

As *Il2rg*$^{-/-}$*Rag2*$^{-/-}$ mice lack T and B cells in addition to NK cells, we sought to determine if the absence of NK cells alone explained the observed reduction in acute lung injury during PGD. We adoptively transferred 1x10^6 wildtype C57BL/6 NK cells isolated via negative selection into immunodeficient mice 5 days preceding hilar clamp experiments. NK cell repopulation of the lung and splenic niches were confirmed via flow cytometry (Supplemental Figure 3). Representative H&E histopathology from hilar clamp lungs following NK cell reconstitution are displayed in Figure 3B and demonstrate severe diffuse alveolar damage. We found adoptive transfer of NK cells resulted in increased injury relative to wildtype shams or immunodeficient mice undergoing hilar clamp. (Figure 3C and 3D). As suspected, there was no difference in extravascular fluid volume or gamma counts per gram of dry lung between wildtype mice and adoptive transfer mice following hilar clamp.

NK cells migrate to lung tissue and become activated during experimental IRI

We examined if responding NK cells were intravascular or within the lung tissue at the time of pulmonary IRI using the hilar clamp versus sham experimental model. Four hours following clamp release, PE-conjugated anti-NK1.1 was administered intravenously to mice to pulse label the intravascular NK cells (Figure 4A). Dissociated lung cells were then stained for NKp46 expression to identify total NK cells in the tissue. Figure 4B and 4C demonstrate intravascular and tissue distributions of NK cells among experimental pulmonary IRI and control mice. In mice undergoing sham procedure, NK cells were mostly anti-NK1.1 and anti-NKp46 co-stained, indicating that they were in the intravascular compartment (59% interquartile range [IQR] 57–68%). Following HC procedure, more NK cells had NKp46 staining alone and were within tissue (64% IQR 54–69%) compared to the intravascular compartment.

We then compared NK cell maturation states across the two compartments. Compared to sham, HC animals had a decrease in the proportion of immature NK cells intravascularly, but the immature fraction in the tissue was unchanged (Figure 4D and 4E, with representative flow cytometry dot plots in Supplemental Figure 4). By contrast, the proportion of mature NK cells in the intravascular space was unchanged following HC, but there was a significant increase in mature NK cells in the tissue in HC versus sham (Figure 4F, G). To visualize NK cells within the lung, we performed tissue immunohistochemistry from hilar clamp and sham lungs (Figure 4H). We found NK cells accumulating bronchioles following ischemia-reperfusion injury. Further, within lungs subjected to hilar clamp, it appears that increased extravasated NK cells may even occlude the small bronchioles. Together, these data demonstrate a tissue-specific increase in mature NK cells following hilar clamp and suggest that NK cells are homing from the periphery to the extravascular space surrounding airways.

Pulmonary NK cells exhibit an activated circulating phenotype

To determine if NK cells in the lung expressed tissue-resident or circulating surface markers, we compared NK cells collected from the dissociated lung to those collected from the blood in 2 hilar clamp and 2 sham mice with a 25-parameter spectral flow cytometry panel (Figure 5A). Representative histograms and Uniform Manifold Approximation and Projection (UMAP) heat maps for each marker are displayed in Supplemental Figure 5. Notably, we found no difference in tissue-resident markers, CD69 or CD49a, between blood or lung NK cells (Figure 5B, C). However, lung NK cells had decreased CD62L compared to blood NK cells (Figure 5D). This evidence suggests that the lung NK cells originated from circulating sources. Compared to blood NK cells, lung NK cells had increased CD16 (Figure 5E), KLRG1 (Figure 5F), Ly6c (Figure 5G), and CD11b (Figure 5H) and decreased CD27 (Figure 5I) and DNAM1 (Figure 5J). Together, these differences suggest a more activated phenotype. NK cell KLRG1 ($r = 0.97$, $p = 0.03$) and DNAM1

(r = 0.96, p = 0.04) were positively correlated between lung and blood samples. However, no other markers demonstrated a significant correlation between these compartments.

CD56+ cells are increased in human lung tissue following severe PGD

To determine if NK cells are present within lung tissue during clinical PGD, we identified 7 subjects with severe PGD and 6 subjects without severe PGD for whom biopsy tissue blocks were available for research. Surgical lung biopsies from representative subjects with severe PGD are shown at 3, 5, 20, and 30 days in Figure 6. Biopsies during this critical time after lung transplantation are not routinely performed, but comparison biopsies were obtained from subjects within the first 30 days after transplantation. Baseline characteristics for these subjects are shown in Supplemental Table 1. Figure 6A shows H&E sections with corresponding high power CD56 staining of biopsy tissue. H&E preparations demonstrate PGD injury in all 4 samples with diffuse alveolar damage characterized by edema, diffuse alveolar septal thickening, and type II pneumocyte hyperplasia. CD56 staining reveals abundant CD56+ lymphocytes throughout areas of lung injury. CD3+ and CD56+ cells were quantified per high power field (HPF, Figure 5B and 5C) showing a significantly increased proportion of CD56+ cells relative to CD3+ cells during severe PGD (Figure 5D, p = 0.05).

Severe PGD in humans is associated with increased mature, CD16+ NK cells in bronchoalveolar lavage

To assess if NK cells are associated with clinical PGD, we prospectively collected bronchoalveolar lavage (BAL) fluid from lung transplant recipients within the first 90 days after transplantation during surveillance bronchoscopy. NK cells (CD3-CD56+) were assessed by flow cytometry in fresh BAL from 94 bronchoscopies in 61 individual lung transplant recipients. The characteristics of this group of subjects are shown in Table 1. The frequency of CD16+ NK cells were increased during severe PGD, defined as ≥ grade 2 on post-operative day 2 or 3, compared to other grades of PGD (Figure 6E, $p = 0.02$). Additionally, both the frequency of CD16+ NK cells (Figure 6F) and

absolute numbers of CD16+ NK cells (Figure 6G) were increased with increasing PGD grade on post-operative day 3 after lung transplantation. Representative histograms for markers on CD16- and CD16+ NK cells are displayed in Supplemental Figure 6A. Compared to CD16- NK cells, CD16+ NK cells had less cellular proliferation by Ki67 staining and were more mature as demonstrated by increased Killer Cell Immunoglobulin-like receptor expression and decreased inhibitory NKG2A receptor expression (Supplemental Figure 6B). These data demonstrate that mature NK cells are increased in transplanted lungs for up to 90 days following PGD, similar to the observations reported in experimental models.

NK cells are also increased in an orthotopic lung transplant with prolonged cold ischemia model of IRI

We measured NK cells in orthotopically transplanted lungs following prolonged cold ischemia (OLT-PCI). Compared to the HC model, this model may more closely replicate the conditions of human organ preservation and transplantation (Figure 7A). Consistent with our hilar clamp versus sham experiments, we found increased frequencies of NK cells (CD3-NKp46+) in lungs subjected to OLT-PCI (Figure 7B) as well as increased total NK cells (Figure 7C) relative to native right lungs. We also measured CD8+ T cells, NKp46+ T cells, and myeloid cells in this model. Similarly, we found no differences in frequencies or total counts of these cells in this model (Figure 7D-I).

The majority of NK cells are recipient-derived and peripheral rather than donor-derived or lung-resident in the OLT-PCI model.

To guide the timing and route of potential lung transplant induction strategies targeting NK cells, we determined whether lymphocytes in the injured lung originate from peripheral populations (recipient) or expand from the pulmonary niche (donor). Following 18 hours of cold ischemia, we transplanted lungs from C57BL/6 *Cd45.1* congenic mice into wildtype (*Cd45.2*) C57BL/6 mice using the OLT-PCI model (Figure 7J). NK cell and other lymphocyte origin were identified by CD45 allotype (Figure 7K). For reference, splenic cells were 100% recipient in origin (Figure 7L,

p = 0.008). We found that over 80% of the lymphocytes in the injured lung were of recipient rather than donor origin (Figure 7M). Similarly, 70% of the NK cells in experimental PGD lungs were from the recipient (Figure 7N, 70 IQR 56–77%). Of the donor lymphocytes that were present in the injured lung, 38% were NK cells (Figure 7O, p = 0.03) as compared with 9% of recipient lymphocytes. Thus, while donor NK cells are enriched in the allograft, the majority of NK cells in the allograft following OLT-PCI are recipient derived.

Acute lung injury is abrogated with NK cell depletion preceding experimental IRI.

As a preclinical mouse model of an NK cell cytoreduction strategy, NK cells were depleted with anti-NK1.1 monoclonal antibody in both donor and recipient C57BL/6 mice preceding OLT-PCI (Figure 8A). This strategy successfully depleted pulmonary NK cells in the anti-NK1.1 group compared to isotype-matched control Ig-treated lungs (Figure 8B). Mice treated with depleting antibodies had significantly less injury measured by arterial oxygen (Figure 8C), total left lung BAL protein (Figure 8D), and left lung BAL neutrophils (Figure 8E) following OLT-PCI compared to controls. Figure 8F demonstrates attenuated injury in representative H&E images from a mouse subjected to OLT-PCI after receiving anti-NK1.1 antibody relative to an animal that received isotype control. This demonstrates that treatment strategies targeting NK cells may reduce PGD-associated acute lung injury.

Stress molecules are increased on pulmonary epithelial and endothelial cells during experimental IRI.

At homeostasis, endothelial and epithelial cells express minimal stress molecules. Under the pressure of hypoxia, HIF-1α induction leads to rapidly increased endothelial and epithelial stress molecule surface expression (12). This phenomenon has not been investigated during pulmonary ischemia-reperfusion injury, but we hypothesized that the mouse stress-induced NKG2D ligands, MULT1 and RAE-1, would be increased within the lung following hilar clamp injury. We measured stress ligands on epithelial and endothelial populations within the dissociated mouse lung (Figure

9A – E). We observed an increased percentage of epithelial cells expressing MULT1 (Figure 9F, p = 0.03), and increased MULT1 median fluorescent intensity on epithelial cells (Figure 9E, p = 0.0002) following hilar clamp injury. Similarly, RAE-1 was increased on epithelial cells as a percentage (Figure 9G, p = 0.001) and by MFI (Figure 9H). For endothelial cells, MULT1 expression was low and there were no statistically significant differences in the percentage of endothelial cells expressing the molecule or MFI of MULT1 (Figure 9I and 9J, p = 0.08 and p=0.2). RAE-1 was increased during acute injury by both metrics on endothelial cells (Figure 9L, percentage of cells, p = 0.004; Figure 9M, MFI, p = 0.03).

Acute lung injury is abrogated in the absence of NKG2D signaling during experimental IRI.

Upon binding to stress molecules via the NKG2D receptor, DAP10 and DAP12 signaling lead to potent NK cell activation. Given our observations of increased NK cell NKG2D and increased pulmonary parenchymal cell stress ligands, we hypothesized that NKG2D ligation is the major activating signal for NK cells following ischemia-reperfusion injury. Figure 9N depicts the 4 experimental groups used to investigate the NKG2D receptor as an activating signal in the hilar clamp versus sham model. To determine if NKG2D ligation was the integral activating single, we dosed animals with a non-depleting antibody against the NKG2D receptor or an isotype-matched control antibody on days -7 and -1 preceding hilar clamp procedures. To determine if the NKG2D receptor on NK cells, versus other NKG2D expressing cells, was mediating this interaction, we adoptively transferred NK cells from mice lacking the NKG2D receptor (*Klrk1*$^{-/-}$) or from wildtype C57BL/6 into immunodeficient mice (*Il2rg*$^{-/-}$*Rag2*$^{-/-}$) 5 days preceding hilar clamp. In animals with NKG2D antibody blockade or NK cells lacking the NKG2D receptor, we found reduced extra vascular lung water (Figure 9O) compared to the two control groups. Similarly, there was a reduction in radiolabeled albumin detected in the lungs of mice that received anti-NKG2D or *Klrk1*$^{-/-}$ NK cells (Figure 9P). Finally, we found significantly decreased endothelial cell permeability in

the group receiving anti-NKG2D monoclonal antibody (Figure 9Q). These results demonstrate that the NKG2D receptor contributes to ischemia-reperfusion injury that is driven by NK cells.

Discussion

Together, these data demonstrate a central role for NK cells in acute lung injury resulting from ischemia, hypoxia, and reperfusion. Under the stress of experimental IRI, we observed upregulation of stress molecules on endothelial and epithelial cells and evidence of activated NK cells trafficking from the periphery to lung tissue in mouse models and human tissue samples. We demonstrate that these NK cells are cytotoxic and sufficient for the lung injury of pulmonary IRI. Our finding that NK cell depletion abrogated acute lung injury due to experimental IRI, suggests that NK cells have potential as therapeutic targets. We further identify a plausible specific target, the NKG2D receptor.

Our data suggest that a dominant mechanism for this interaction is NK cell recognition via NKG2D of epithelial and endothelial stress molecules within the lung. These stress molecules which are ligands for the NKG2D receptor, have been shown to be increased in the lung or on pulmonary epithelium during idiopathic pulmonary fibrosis, exposure to tobacco smoke, and with acute infection (20-22). While additional mechanisms of NK cell activation, such as through the NKp46 receptor, may contribute to IRI injury (23), our finding that targeted NKG2D genetic depletion and NKG2D blockade reduce experimental PGD injury suggest that NKG2D antibody blockade may be useful as a potential human therapy. Indeed, an analogous monoclonal anti-NKG2D antibody is currently undergoing phase II clinical trials for the treatment of inflammatory bowel disease (24). We observed an increase in NKG2D on NK cells in our 4-hour injury model with hilar clamp. This was somewhat surprising as NKG2D is reported to be endocytosed following ligation via DAP10/12-dependent mechanisms (25) and NKG2D is downregulated on NK cells with constitutive stress ligand signaling, (26). However, this initial increase in NKG2D might reflect an

influx of activated circulating NK cells. We note that with longer NKG2D-ligand interaction time, as occurs in the OLT-PCI model, there was relatively less NKG2D observed on NK cells.

NK cells are attractive targets for novel therapeutics in transplantation. NK cell receptors are somatically encoded and not shared on many other significant immune cell subsets. At the same time, they have a potential to profoundly impact transplant-related lung injury, because their IFN transcripts and cytotoxic granules are abundant and preformed, rendering them resistant to induction immunosuppressants (27, 28). There also is evidence that they may become even more activated by scavenging IL2 in the setting of IL2 receptor blockade (29).

We found that significant proportion of lymphocytes and NK cells in the injured lung are of recipient or peripheral origin. Intravascular pulse labeling experiments and tissue immunohistochemistry demonstrate that most of these NK cells are within the injured lung tissue rather than the intravascular space. Given the rapid time course and predominantly recipient origin, most NK cells appear to be homing to the allograft, rather than proliferating locally. Donor-derived NK cells may originate from transplanted lymphoid tissue. Further, these IRI-associated NK cells have more activated, mature phenotypes and lack tissue-specific markers. Overall, these findings are consistent with NK cell behavior in viral infections and suggest a conserved response by NK cells to lung tissue injury across etiologies (30). We found decreased PE-labeled NK cells in the injured lungs, and we believe this approach accurately assessed the NK cell compartment as injured tissue may be more permeable to PE-labeled anti-NK1.1. Interestingly, the injury phenotype appeared somewhat accentuated in adoptive transfer experiments. This increased injury may indicate that NK cells are activated during adoptive transfer with unopposed proliferation in the relatively empty pulmonary niche. One outstanding question is how NK cells may traffic to sites of injury. Soluble stress ligands may serve as NK cell chemokines (31). NK cells may also be responding to chemokines associated with PGD, via chemokine receptors CCR2, CCR5, and CXCR3 (32, 33).

The major mechanism of injury appeared to be direct cytotoxicity, given evidence of cytotoxic degranulation without changes in intracellular cytokine levels. Nonetheless, we did not examine stimulated cytokine release and this remains a potential mechanism, as NK cells are potent recruiters and activators of other immune cells through chemokine secretion (34). NK cells can also mediate sterile lung injury induced with lipopolysaccharide via neutrophil recruitment (35). Several studies of experimental and human PGD have described the importance of neutrophils, via neutrophil-derived extracellular traps (NETs), as well as macrophages in mediating PGD lung injury (8, 36, 37). Chemokine release may recruit neutrophils and bridge the role of NK cells with our prior finding of NET-mediated PGD injury (8, 38).

In human lung transplant BAL, we found that CD16+ NK cells were increased in absolute and relative quantities for up to 90 days following severe PGD. CD16 is an activating Fc receptor that initiates antibody-dependent cell-mediated cytotoxicity (ADCC) (39) as well as a marker of NK cell maturation. Lung-restricted autoantibodies have been shown to mediate experimental PGD and are significant risk factors for clinical PGD (40-42). These are not part of routine pre-transplant screening, but in one series of 142 lung transplant recipients, up to 30% of subjects had at least one lung-restricted autoantibody (36). Together, these data suggest that ADCC from donor-specific alloantibodies or lung-restricted autoantibodies may be another potential mechanism for NK cell injury in PGD.

A significant strength of this study is the concordant findings from two separate animal models of PGD paired with associations among a single-center human lung transplant cohort. Nonetheless, this work has some limitations: obtaining tissue samples early in subjects in the post-transplant period is not feasible as these patients can be critically ill and subject to increased risk from invasive sampling. Subjects with PGD often have less early invasive surveillance bronchoscopies for this reason, which would be expected to bias our human BAL findings towards the null hypothesis. Results from a single-center human study are subject to variability from differences

in transplant protocols and heterogeneity in subject characteristics. While we show NK cell-specific effects, we cannot exclude the possibility that a small number of innate lymphoid cells may participate (Supplemental Figure 7L) (43). A recent study of donor lung tissue before and after reperfusion showed a steep decline in highly immature NK cells in lungs ($CD3^-CD11b^-CD11c^-CD56^+$) preceding PGD, which indirectly supports our findings here (44).

Our findings may have broader implications, as NK cells can play multiple important roles in the context of lung transplantation (45). In addition to the effects observed on IRI, NK cells appear to impact CLAD outcomes both through immune surveillance of CMV (46) and depletion of host antigen-presenting cells (47). While NK cell depletion could increase infection or rejection risks, targeting NK-associated receptors most associated with ischemia reperfusion injury, such as NKG2D, could ameliorate this concern. One outstanding question is whether potential treatment should be targeted within the donor organ or as part of the recipient induction regimen. Our finding that NK cells are mostly recipient-derived would suggest adding an NK cell inhibitory therapy to induction protocols may be beneficial.

In summary, we describe a novel role for NK cells in experimental IRI and lung PGD, which implicates the NKG2D receptor as a potential therapeutic target that could improve outcomes following lung transplantation.

Methods

Mice

Male mice aged 8 to 12 weeks and weighing 28-30 grams were housed in a pathogen-free barrier facility for all experiments. C57BL/6J and CD45.1 (B6.SJL-*Ptprc*^{a}*Pepc*^{b}/BoyJ) congenic animals were purchased from Jackson Laboratories (#002014, Bar Harbor, ME). *Il2rg*$^{-/-}$*Rag2*$^{-/-}$ constitutive double knock-out C57BL/6 mice (*C57BL/6NTac; B10(Cg)Rag2*^{tm1Fwa} *Il2rg*^{tm1Wjl}) were purchased from Taconic (4111-M), and C57BL/6 *Klrk1*$^{-/-}$ mice were derived as previously

described (26). All experiments were conducted according to UCSF Institutional Animal Care Use Committee-approved protocols.

Experimental models of pulmonary ischemia-reperfusion injury

Details regarding methods of experimental pulmonary IRI models have been previously published (8, 38). Mouse procedures were performed by a surgeon with microvascular training. For the hilar clamp (HC) model, mice underwent left thoracotomy to expose the hilar structures. A silk suture was tied in a slipknot or left untied in a sham (S) surgery. Mice were extubated and monitored until complete recovery from anesthesia. Following a 2-hour period of ischemia, the suture was removed, and animals were euthanized after 4-hours of warm reperfusion. In a series of experiments, 20 ug of PE-conjugated anti-NK1.1 (clone PK136, BioLegend, San Diego, CA, #108708) in sterile PBS was injected retro-orbitally in anesthetized mice 10 minutes prior to euthanasia. Lungs were collected, dissociated, and NK cells were analyzed by flow cytometry.

Orthotopic left lung transplantations in mice with prolonged cold ischemia (OLT-PCI) of the donor organ were performed as previously reported (8, 48). The left donor lung was air-inflated, infused with Perfadex (XVIVO Perfusion Inc., Englewood, CO), and stored at 4^{o}C for 18 hours while wrapped in Perfadex-soaked gauze. The donor organ was implanted using a plastic cuff for anastomosis. The recipient animal was euthanized 8 hours after transplantation. The left and right lungs, as well as blood, were collected for analysis.

In selected experiments, B6 *Cd45.1* mouse lungs (B6.SJL-*Ptprc*^{a}*Pepc*^{b}/BoyJ) were transplanted into C57BL/6 recipients following prolonged cold ischemia. NK cells of CD45.1 or CD45.2 allotype origin were enumerated by flow cytometry in dissociated lung and spleen. Dissociated native and uninjured lungs were used as internal flow cytometry controls.

NK cell depletion and NKG2D blockade

C57BL/6 donor and recipient mice were injected intraperitoneally (IP) with 200 ug anti-NK1.1 monoclonal antibody (clone PK136, American Type Culture Collection, Manassas, VA, #HB-191) or isotype-matched control antibody (anti-rat, gp42, clone 3G7, provided by Dr. Mary Nakamura, San Francisco CA) at 7 days and 24 hours preceding surgery (49). For hilar clamp experiments, C57BL/6 mice were injected with 200 ug anti-NKG2D monoclonal antibody (clone CX5, UCSF antibody core, San Francisco, CA, #AM053-PURE) or isotype-matched control antibody (rat IgG1, clone HRPN, UCSF antibody core, San Francisco, CA, #AM047-PURE) at 7 days and 24 hours preceding hilar clamp procedures.

Acute lung injury measurements

Wet-to-dry lung weights, lung vascular permeability to ^{125}I-labeled albumin (Iso-Tex Diagnostics) delivered i.v. and extravascular lung water were measured as previously described (8). Arterial blood partial pressure of Oxygen (PaO_2) was assessed after mice were first anesthetized with 0.6 mg/kg ketamine and 0.1 mg/ml xylazine intraperitoneally. Anterior tracheotomy was performed, and animals were supported with 100% O_2 as previously described (8). After 5 minutes, arterial blood was collected via left ventricular puncture and PaO2 was measured with an i-STAT® 1 Handheld Analyzer and VetScan CG4 i-STAT Cartridges (Abaxis, #89126). Additionally, single left lung lavage with saline was performed, and total protein and neutrophils were measured (8).

To visualize lung injury, mice were euthanized following IRI procedures. The lungs were inflated with air, and the bronchus was tied off with silk suture. The inflated lung was excised from the chest cavity and placed into 10% neutral buffered formalin for 48 hours, then transferred to 70% ethanol. The lungs were embedded in paraffin, sectioned and stained with Hematoxylin and Eosin (H&E). Slide images were acquired with an Olympus BX51 microsocope at 4X and 20X magnifications using a digital camera (Diagnostic Instruments, DBX) and commercial imaging software (Bioquant Life Science 2013 v13.5.60).

Lung digestion

To isolate cells from harvested lungs, the left lungs were added to a solution containing 1 ml of PBS with 0.05 mg/ml Liberase TM (Sigma-Aldrich, #5401119001) and 10 µl of 10 µg/µl DNAse I (Sigma-Aldrich, #10104159001). The lungs were cut with scissors into 1 mm pieces and incubated in a shaking incubator for 1 hour at 37°C. The incubated lungs were strained through a 40-µm mesh nylon filter using 10 ml of PBS and pelleted for 5 minutes at 4°C.The samples were resuspended in 2 ml of PBS and 2 ml of ACK Lysis Buffer (Gibco, #A10492) for 5 minutes at room temperature, then pelleted for 5 min at 4°C. Each sample was then washed and re-suspended in flow cytometry buffer.

Mouse Lung Immunophenotyping

Following collagenase digestion, suspended cells were washed and incubated at room temperature with anti-mouse anti-CD16/CD32 to block non-specific binding and stained with viability dye (Fixable Viability Dye eFluor506, eBioscience #65-0866-14). Lymphocyte subsets were identified using Alexa Fluor700-conjugated anti-CD45 (clone# 30-F11, BD Biosciences #560510), APC-conjugated anti-CD3 (clone# 17A2, BioLegend #100235), PE-Cy7-conjugated anti-CD8 (clone# 53-6.7, BioLegend #100721). NK cell subsets were identified using FITC-conjugated anti-CD335 (NKp46) (clone# 29A1.4, BioLegend #137606), PE-conjugated anti-CD314 (NKG2D) (clone# CX5, BioLegend #130207), PerCP-conjugated anti-CD27 (clone #LG.7F9, Invitrogen #46-0271-80), and V450-conjugated anti-CD11b (clone# M1/70, BD Biosciences #560456). For intracellular cytokine measurements in NK cells, lung cells were prepared with permeabilization and fixation buffers per manufacture protocol (BD Biosciences, #554714). Alexa Fluor 647-conjugated anti-IFNγ (clone# XMG1.2, BioLegend #505816) and PE-Dazzle 594-conjugated anti-TNFα (clone# MP6-XT22, BioLegend #506345) stains were applied with representative histograms displayed in Supplemental Figure 2. The core panel and gating strategy are shown in Supplemental Figure 7. A separate NK cell degranulation panel employed V450-conjugated anti-CD107a (clone #1D4B, BD Biosciences # 560648). Samples were acquired

with a Beckman Coulter Navios cytometer (50). Negative thresholds were set based on fluorescence minus one and unstained controls. Antibody staining was quantified by median fluorescent intensity (MFI) and visualized by logarithmically scaled histogram plots. Viable lymphocytes were identified by e506^{-}CD45^{+} expression in addition to forward and side light scatter profiles. NK cells were identified as CD3^{-}NKp46^{+}. Intravascular NK cells were identified as CD3^{-} NKp46^{+}NK1.1^{+} and NK cells in lung tissue, which would not be stained with the injected PE-conjugated anti-NK1.1 mAb, were identified as CD3^{-}NKp46^{+}NK1.1^{-} (51). The antibody conjugates, data acquisition, and gating strategy for the spectral flow cytometry experiments are detailed in the supplemental methods and Supplemental Figure 8. CD45+CD3-NKp46+ NK cells are highlighted in in this extended panel, which was designed to exclude innate lymphoid, T and B cells.

Tissue Immunofluorescence

Fixed lung cryosections were prepared as previously described (52). Off-target binding was blocked with 10% normal donkey serum with 0.3% BSA in staining buffer (0.3% Triton X-100 in PBS), and samples were incubated overnight with primary antibodies raised against NKp46 (goat polyclonal, #AF2225, R&D) or CD31 (rabbit monoclonal D8V9E, #77699S, Cell Signaling Technology). Samples were washed, and then incubated overnight with Alexa Fluor 488-conjugated donkey anti-goat IgG (polyclonal, Jackson ImmunoResearch, #705-545-147) and Cy3-conjugated donkey anti-rabbit IgG (polyclonal, Jackson ImmunoResearch , #711-166-152) in staining buffer. After a final wash, samples were mounted in Vectashield (#H-1000, Vector Labs) + 50 µg/ml DAPI. Lung sections were imaged using a 20× oil immersion objective on an SP5 confocal microscope (Leica).

NK cell isolation and adoptive transfer

NK cells from C57BL/6 mice were adoptively transferred into *Il2rg*$^{-/-}$*Rag2*$^{-/-}$ mice according to previously published protocols (53). Briefly, 8-week-old C57BL/6 mice were euthanized according to institutional protocol. With sterile technique, the spleen was removed and dissociated through a 40-μm mesh nylon filter (Fisher Scientific, #22363547) in 0.1% bovine serum albumin (BSA) in sterile saline. The isolated splenocytes were counted using an automated Countess II FL cell counter (Invitrogen) and concentrated to 1x10^{8} cells/mL. NK cells were isolated from splenocytes via negative magnetic selection (StemCell Technologies, #19855). NK cells (1x10^{6} in 200 μL sterile PBS) were injected intraperitoneally (i.p.) into *Il2rg*$^{-/-}$*Rag2*$^{-/-}$ mice and allowed to expand *in vivo* for 5 days prior to experiments. NK cell expansion was confirmed via flow cytometry. Supplemental Figure 3 compares NK cell phenotypes among wildtype lung and spleen and 5 days following adoptive transfer.

Human Subjects

Seven clinical cases of severe PGD were identified with surgical lung biopsies within the first 30 days following lung transplantation. Six clinical cases of routine lung transplant surveillance bronchoscopies in subjects with no PGD were selected as negative controls. Formalin-fixed and paraffin-embedded samples were recut and stained in separate sections with H&E, anti-CD56 (clone CD564, Leica Biosystems, #PA0192), and anti-CD3 (clone LN10, Leica Biosystems, #PA0122). Cells of interest were quantified in 20 high powered fields (HPF, 20x magnification) for each sample and repeated. Bronchoalveolar lavage fluid (BAL) was prospectively collected and analyzed as part of routine clinical care for subjects who underwent lung transplantation between 11/2013 and 4/2016. We included all consenting adult subjects who received single lung, bilateral lung, or heart-lung allografts at UCSF and received at least one adequate BAL sample within the first 3 months following transplantation. Samples were considered adequate if at least 50 NK cells were identified by flow cytometry. Our institution performs bronchoscopy with lavage and transbronchial biopsies as part of routine surveillance at 0.5, 1, 2, and 3 months after

transplantation. Additional bronchoscopies are performed when clinically indicated for suspicion of acute infection or rejection. Primary graft dysfunction was graded for all subjects according to international criteria (7). Subject clinical data were obtained by chart review of UCSF records and from the United Network for Organ Sharing (UNOS) database. Standard post-transplant induction regimens for all subjects included methylprednisolone, mycophenolate mofetil, and 20 mg intravenous basiliximab intraoperatively and on post-operative day 4. Initial maintenance immunosuppressant therapy included tacrolimus, prednisone, and mycophenolate mofetil.

Human BAL Immunophenotyping

NK cells from fresh BAL samples were phenotyped as described previously (46, 54). Each sample was treated with human aggregated immunoglobulins to block non-specific binding and stained with viability dye (eBioscience, South San Francisco, CA, #65-0863-18). NK cell subsets were identified using: Allophycocyanin (APC)-conjugated anti-NKG2A(clone # 131411, R&D Systems, Minneapolis, MN, #FAB1059A), R-phycoerythrin (PE)-conjugated anti-KIR2D (clone NKVFS1, Miltenyi Biotec, San Diego, CA, #130- 092-688), PE-conjugated anti-KIR3D (clone Z27.3.7, Beckman Coulter, Brea, CA, #IM3292), peridinin-chlorophyll-protein complex (PerCP)-conjugated anti-KIR3DL1 (clone DX9, BioLegend, San Diego, CA, #312718), PE-Cy7-conjugated anti-CD56 (clone HCD56, BioLegend, #318318), Alexa Fluor700-conjugated anti-CD45 (clone HI30, BioLegend, #304024), and allophycocyanin-cyanine 7 (APC-Cy7)-conjugated anti-CD3 (clone SK7, BioLegend #344818). Samples were acquired with a Beckman Coulter Navios cytometer and data were analyzed with the Kaluza software package (Beckman Coulter). Negative thresholds were set based on no-fluorochrome controls. The gating strategy for human BAL specimens are displayed in Supplemental Figure 8. Viable lymphocytes were identified by viability dye exclusion, $CD45^+$ expression, and forward and side light scatter profiles. NK cells were identified as $CD56^+CD3^-$.

Statistical analysis

Outcome variable distributions were assessed for normality visually and with the Shapiro-Wilks test. Parametric data were analyzed using a 2-tailed unpaired Student's t-test, and 2-tailed Mann-Whitney U tests were applied for non-parametric data. A P value less than 0.05 was considered significant. Comparisons of means in experiments with multiple groups were made with Kruskal-Wallis test, and Dunn's test was used to assess *post-hoc* differences. Comparisons between lung and peripheral blood NK cell phenotypes were made with a paired Student's t-test and Pearson's correlation coefficient. Results were visualized using box and whisker plots showing individual data points bound by boxes at 25^{th} and 75^{th} percentiles and medians depicted with bisecting lines.

For the human BAL data, the association between NK cells and PGD grade as a dependent ordinal variable on post-operative day 3 was determined using cumulative linked mixed model (CLM) regression analysis to account for repeat measures among individual subjects. Differences between NK cell surface markers in BAL were determined with paired Student's t-tests.

Differences between CD16 genotype and PGD as a binary variable was determined with generalized linear models adjusted for transplant characteristics known to cause genetic variation or to impact early outcomes: recipient age, transplant type, transplant indication, sex, and ethnicity.

For all analyses, a p-value <0.05 was considered significant. Statistical analyses and visualization were performed in R (R Foundation for Statistical Computing, Vienna, Austria) using packages "mgcv," "ordinal," "ggplot," "stringr," "multcomp," "ggbeeswarm," and "ggpubr."

Study Approval

The UCSF institutional review board approved the human subject components of this study under protocol 13-10738. Written and informed consent was obtained from all participants prior to inclusion in this study. All animal procedures and experiments were conducted according to UCSF Institutional Animal Care Use Committee-approved protocols.

Acknowledgements

We thank William Karlon, Chiyo Uchida, Brandon Lim, Ryan Tsiao, Brandon Cowan, and Malori Mindo for instrumental aid in collecting and processing study samples. We also thank Mary Ellen Kleinhenz, Lorianna Leard, Rupal Shah, Nicholas Kolaitis, Aida Venado and the other members of the clinical lung transplant team for their care of our patients and design of the clinical protocols. We are thankful for the cooperation of Donor Network West, for all of the organ and tissue donors, and their families for giving gifts of life and knowledge with their generous donation.

This project was funded with support from the UCSF Nina Ireland Program for Lung Health (NIPLH) Innovative Grant program (JRG), VA ORD CX002011 (JRG), the Joel D. Cooper Award from the International Society for Heart and Lung Transplantation (DRC), the Cystic Fibrosis Foundation Harry Shwachman Career Development Award CALABR19Q0 (DRC), and NHLBI HL151552 (JRG) & HL130324 (MRL). LLL is supported in part by the Parker Institute for Cancer Immunotherapy and NIH AI068129 and OAA is a CRI-Irvington Postdoctoral Fellow. We acknowledge the PFCC (RRID:*SCR 018206*) supported in part by Grant NIH P30 DK063720 and by the NIH S10 Instrumentation Grant S10 1S10OD026940-01.

Authorship Contributions: Study design: DRC, JRG, LLL, MRL, SRH; Experiments: DRC, EA, BM, PW, MN, SC, OAA; Analysis of results: DRC, JRG, OAA, DD, JPS; Vital data/interpretation: DRC, JRG, MN, LLL; Manuscript preparation: DRC and JRG with input from all authors.

Competing Interests Statement: LLL and UCSF have licensed intellectual property rights regarding NKG2D for therapeutic applications. The authors have no other relevant financial relationships to disclose.

References

1. Lund LH, et al. The Registry of the International Society for Heart and Lung Transplantation: Thirty-fourth Adult Heart Transplantation Report; Focus Theme: Allograft ischemic time. *J Heart Lung Transplant.* 2017;36(10):1037-46.

2. Oto T, et al. Association between primary graft dysfunction among lung, kidney and heart recipients from the same multiorgan donor. *Am J Transplant.* 2008;8(10):2132-9.

3. Christie JD, et al. The effect of primary graft dysfunction on survival after lung transplantation. *Am J Respir Crit Care Med.* 2005;171(11):1312-6.

4. Daud SA, et al. Impact of immediate primary lung allograft dysfunction on bronchiolitis obliterans syndrome. *Am J Respir Crit Care Med.* 2007;175(5):507-13.

5. Siegleman SS, et al. Pulmonary reimplantation response. *Ann Surg.* 1973;177(1):30-6.

6. Matute-Bello G, et al. Animal models of acute lung injury. *Am J Physiol Lung Cell Mol Physiol.* 2008;295(3):L379-L99.

7. Snell GI, et al. Report of the ISHLT Working Group on Primary Lung Graft Dysfunction, part I: Definition and grading; A 2016 Consensus Group statement of the International Society for Heart and Lung Transplantation. *J Heart Lung Transplant.* 2017;36(10):1097-103.

8. Sayah DM, et al. Neutrophil extracellular traps are pathogenic in primary graft dysfunction after lung transplantation. *Am J Respir Crit Care Med.* 2015;191(4):455-63.

9. den Hengst WA, et al. Lung ischemia-reperfusion injury: a molecular and clinical view on a complex pathophysiological process. *Am J Physiol Heart Circ Physiol.* 2010;299(5):H1283-99.

10. Cooper GE, et al. Human CD49a(+) Lung Natural Killer Cell Cytotoxicity in Response to Influenza A Virus. *Front Immunol.* 2018;9:1671.

11. Vivier E, et al. Innate or adaptive immunity? The example of natural killer cells. *Science.* 2011;331(6013):44-9.

12. Raulet DH, et al. Regulation of ligands for the NKG2D activating receptor. *Annu Rev Immunol.* 2013;31:413-41.

13. Feng L, et al. The effect of renal ischemia-reperfusion injury on expression of RAE-1 and H60 in mice kidney. *Transplant Proc.* 2006;38(7):2195-8.

14. Zhang Z-X, et al. NK Cells Induce Apoptosis in Tubular Epithelial Cells and Contribute to Renal Ischemia-Reperfusion Injury. *J Immunol.* 2008;181(11):7489-98.

15. Zingoni A, et al. Natural Killer Cell Response to Chemotherapy-Stressed Cancer Cells: Role in Tumor Immunosurveillance. *Front Immunol.* 2017;8:1194.

16. Chen GE, et al. Toll-like receptor 4 engagement contributes to expression of NKG2D ligands by renal tubular epithelial cells. *Nephrol Dial Transplant.* 2011;26(12):3873-81.

17. Victorino F, et al. Tissue-Resident NK Cells Mediate Ischemic Kidney Injury and Are Not Depleted by Anti-Asialo-GM1 Antibody. *J Immunol.* 2015;195(10):4973-85.

18. Abel AM, et al. Natural Killer Cells: Development, Maturation, and Clinical Utilization. *Front Immunol.* 2018;9(1869).

19. Alter G, et al. CD107a as a functional marker for the identification of natural killer cell activity. *J Immunol Methods.* 2004;294(1-2):15-22.

20. Aquino-Galvez A, et al. MICA polymorphisms and decreased expression of the MICA receptor NKG2D contribute to idiopathic pulmonary fibrosis susceptibility. *Hum Genet.* 2009;125(5-6):639-48.

21. Wesselkamper SC, et al. NKG2D Is Critical for NK Cell Activation in Host Defense Against Pseudomonas aeruginosa Respiratory Infection. *J Immunol.* 2008;181(8):5481-9.

22. Borchers MT, et al. Sustained CTL activation by murine pulmonary epithelial cells promotes the development of COPD-like disease. *J Clin Invest.* 2009;119(3):636-49.

23. Barrow AD, et al. The Natural Cytotoxicity Receptors in Health and Disease. *Front Immunol.* 2019;10:909.

24. Vadstrup K, and Bendtsen F. Anti-NKG2D mAb: A New Treatment for Crohn's Disease? *Int J Mol Sci.* 2017;18(9).

25. Molfetta R, et al. Regulation of NKG2D-Dependent NK Cell Functions: The Yin and the Yang of Receptor Endocytosis. *Int J Mol Sci.* 2017;18(8):1677.

26. Guerra N, et al. NKG2D-deficient mice are defective in tumor surveillance in models of spontaneous malignancy. *Immunity.* 2008;28(4):571-80.

27. Wang H, et al. The unexpected effect of cyclosporin A on CD56+CD16- and CD56+CD16+ natural killer cell subpopulations. *Blood.* 2007;110(5):1530-9.

28. Wasik M, et al. Effect of FK506 versus cyclosporine on human natural and antibody-dependent cytotoxicity reactions in vitro. *Transplantation.* 1991;51(1):268-70.

29. Martin JF, et al. An IL-2 paradox: blocking CD25 on T cells induces IL-2-driven activation of CD56(bright) NK cells. *J Immunol.* 2010;185(2):1311-20.

30. Lehmann MH, et al. CCL2 expression is mediated by type I IFN receptor and recruits NK and T cells to the lung during MVA infection. *J Leukoc Biol.* 2016;99(6):1057-64.

31. Champsaur M, and Lanier LL. Effect of NKG2D ligand expression on host immune responses. *Immunol Rev.* 2010;235(1):267-85.

32. Frick AE, et al. Early protein expression profile in bronchoalveolar lavage fluid and clinical outcomes in primary graft dysfunction after lung transplantation. *Eur J Cardiothorac Surg.* 2020.

33. Hoffman SA, et al. Plasma cytokines and chemokines in primary graft dysfunction post-lung transplantation. *Am J Transplant.* 2009;9(2):389-96.

34. Li F, et al. Natural Killer Cells Are Involved in Acute Lung Immune Injury Caused by Respiratory Syncytial Virus Infection. *J Virol.* 2012;86(4):2251.

35. Hoegl S, et al. NK cells regulate CXCR2+ neutrophil recruitment during acute lung injury. *J Leukoc Biol.* 2017;101(2):471-80.

36. Bharat A, et al. Antibodies to Self-Antigens Predispose to Primary Lung Allograft Dysfunction and Chronic Rejection. *Ann Thorac Surg.* 2010;90(4):1094-101.

37. Shah RJ, et al. Plasma monocyte chemotactic protein-1 levels at 24 hours are a biomarker of primary graft dysfunction after lung transplantation. *Transl Res.* 2012;160(6):435-42.

38. Mallavia B, et al. Mitochondrial DNA Stimulates TLR9-Dependent NET Formation in Primary Graft Dysfunction. *Am J Respir Cell Mol Biol.* 2019.

39. Wu J, and Lanier LL. *Adv Cancer Res*. Academic Press; 2003:127-56.

40. Bharat A, et al. Lung-Restricted Antibodies Mediate Primary Graft Dysfunction and Prevent Allotolerance after Murine Lung Transplantation. *Am J Respir Cell Mol Biol.* 2016;55(4):532-41.

41. Kaza V, et al. Pre-existing self-reactive IgA antibodies associated with primary graft dysfunction after lung transplantation. *Transpl Immunol.* 2020:101271.

42. Bharat A, and Kreisel D. Immunopathogenesis of Primary Graft Dysfunction After Lung Transplantation. *Ann Thorac Surg.* 2018;105(3):671-4.

43. Verrier T, et al. Phenotypic and Functional Plasticity of Murine Intestinal NKp46+ Group 3 Innate Lymphoid Cells. *J Immunol.* 2016;196(11):4731-8.

44. Monticelli LA, et al. Lung Innate Lymphoid Cell Composition Is Altered in Primary Graft Dysfunction. *Am J Respir Crit Care Med.* 2020;201(1):63-72.

45. Calabrese DR, et al. Natural killer cells in lung transplantation. *Thorax.* 2019;74(4):397-404.

46. Calabrese DR, et al. NKG2C natural killer cells in bronchoalveolar lavage are associated with cytomegalovirus viremia and poor outcomes in lung allograft recipients. *Transplantation.* 2018.

47. Greenland JR, et al. HLA Mismatching Favoring Host-Versus-Graft NK Cell Activity Via KIR3DL1 Is Associated With Improved Outcomes Following Lung Transplantation. *Am J Transplant.* 2017;17(8):2192-9.

48. Okazaki M, et al. A mouse model of orthotopic vascularized aerated lung transplantation. *Am J Transplant.* 2007;7(6):1672-9.

49. Karnbach C, et al. Immune rejection of a large sarcoma following cyclophosphamide and IL-12 treatment requires both NK and NK T cells and is associated with the induction of a novel NK T cell population. *J Immunol.* 2001;167(5):2569-76.

50. Jamin C, et al. Multi-center harmonization of flow cytometers in the context of the European "PRECISESADS" project. *Autoimmun Rev.* 2016;15(11):1038-45.

51. Ruscher R, and Hogquist KA. Intravenous Labeling and Analysis of the Content of Thymic Perivascular Spaces. *Bio-protocol.* 2018;8(5):e2757.

52. Cleary SJ, et al. Complement activation on endothelium initiates antibody-mediated acute lung injury. *J Clin Invest.* 2020.

53. Min-Oo G, and Lanier LL. Cytomegalovirus generates long-lived antigen-specific NK cells with diminished bystander activation to heterologous infection. *J Exp Med.* 2014;211(13):2669-80.

54. Greenland JR, et al. Bronchoalveolar lavage cell immunophenotyping facilitates diagnosis of lung allograft rejection. *Am J Transplant.* 2014;14(4):831-40.

Table 1. Characteristics of the 61 human subjects.

Variable	n
Sex = male	39
Double lung transplant	54
Ethnicity = Caucasian	40
Transplant group	
COPD	7
Cystic Fibrosis	7
Interstitial Lung Disease	47
PGD grade at 72 hours	
0	38
1	10
2	8
3	5

Figure Legends

Figure 1. NK cells are increased in injured lungs from a hilar clamp (HC) model of pulmonary ischemia-reperfusion injury. (A) In the illustrated HC procedure, a slip knot suture is secured around the left hilum and released 2 hours later, followed by 4 hours of *in situ* reperfusion before mice are euthanized. (B) NK cells (CD3-NKp46+) are increased as a percentage of total CD45+ cells (p = 0.008) and in absolute quantity (C, p = 0.04) in dissociated lung tissue following hilar clamp (HC) relative to sham procedures (S). CD3+NKp46+ T cells as a frequency (D, p = 0.1) and by total number of cells (E, p = 0.03) were increased after hilar clamp, but were infrequently identified. CD8+ T cells as a frequency of total lymphocytes (F, p = 0.8) and in total (G, p = 1.0) were not increased after hilar clamp. CD3-NKp46+CD11b+ cells, which are predominantly myeloid (H, p = 0.3; I, p = 0.8) were not different after hilar clamp. All experiments studied at least 5 mice for each condition. Box and whisker plots show individual data points bound by boxes at 25th and 75th percentiles and medians depicted with bisecting lines. Differences were assessed using the Mann-Whitney U test with p<0.05 considered significant.

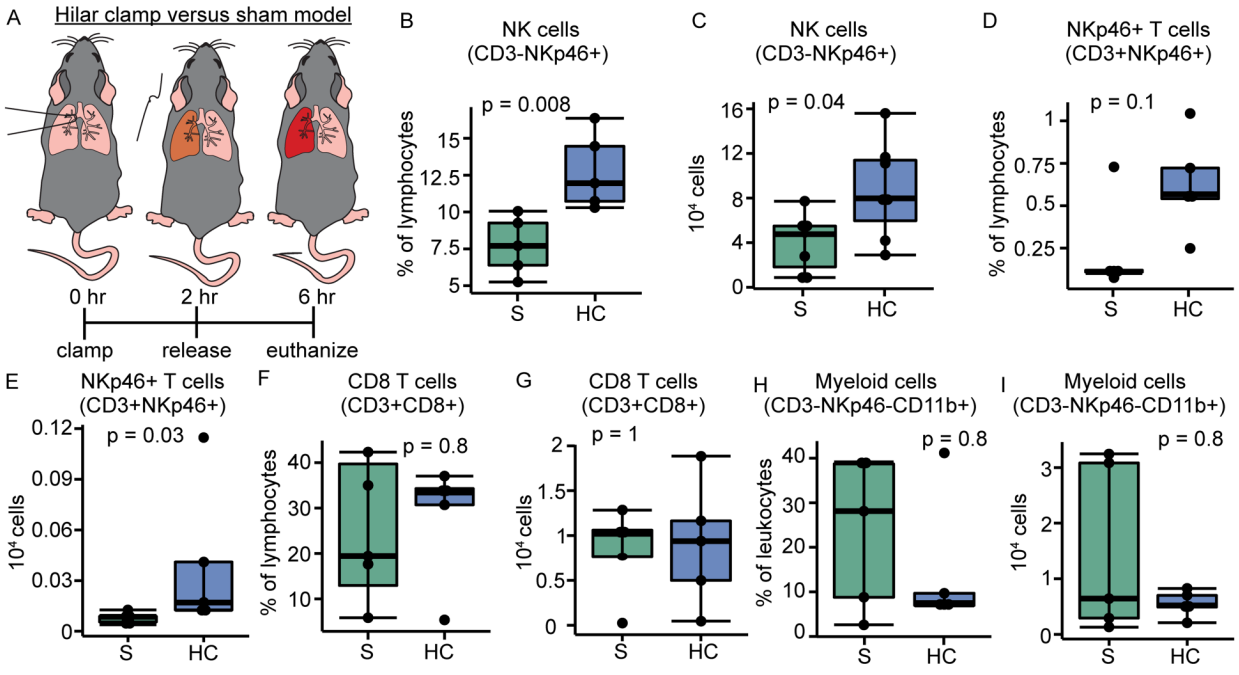

Figure 2. NK cells in acutely injured lungs are more mature, cytotoxic, and activated. (A) As they mature, NK cells (CD3-NKp46+) gain CD27 and then CD11b with the most mature population described as CD27-CD11b+. There were no differences between hilar clamp (HC, n = 5) and sham (S, n = 5) immature NK cell maturation states CD27-CD11b- (B, p = 0.1), CD27+CD11b- (C, p = 0.7), or CD27+CD11b+ (D, p = 0.6). In lungs subjected to hilar clamp, we found increased frequencies of mature (panel E, CD27-CD11b+) NK cells relative to dissociated sham lungs (S, *p* = 0.008). (F) The cytotoxic degranulation marker lysosomal-associated membrane protein (LAMP-1, CD107a) was measured on NK cells, with fluorescence histograms shown, representative of 6 experiments. (G) CD107a+ NK cells were increased following hilar clamp (n = 6) relative to sham (n = 6) procedure (*p* = 0.002), and the mean fluorescence of CD017a was also increased on NK cells (H, *p* = 0.07). (I) The stress ligand receptor, NKG2D, was present on 99% of all NK cells, but had increased surface density after hilar clamp (J, n = 6, *p* = 0.005) compared to sham (n = 6). Box and whisker plots show individual data points bound by boxes at 25th and 75th percentiles and medians depicted with bisecting lines. Differences were determined by the Mann-Whitney U test.

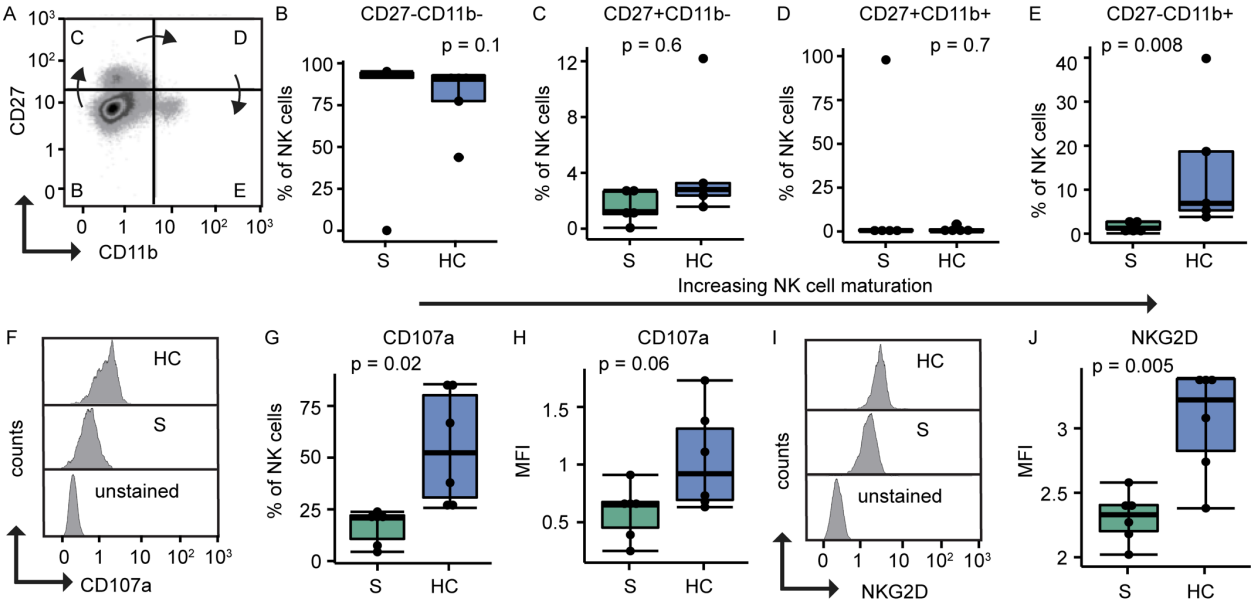

Figure 3. NK cells are sufficient for acute lung injury. (A) *Il2rg*$^{-/-}$*Rag2*$^{-/-}$ mice are deficient in NK, T, and B cells. Five days preceding procedures, NK cells from wildtype C57BL/6 mice were adoptively transferred into *Il2rg*$^{-/-}$*Rag2*$^{-/-}$ C57BL/6 mice. H&E preparations representative of 4 experiments are shown in panel B: wildtype sham (sham), wildtype hilar clamp (C57BL/6 HC), *Il2rg*$^{-/-}$*Rag2*$^{-/-}$ hilar clamp, and *Il2rg*$^{-/-}$*Rag2*$^{-/-}$ with adoptively transferred wildtype NK cells (+NK cells HC) and hilar clamp. The centers for higher magnification locations in 4x images are denoted by "^." Diffuse alveolar damage (DAD), characterized by hyaline membrane formation, intra-alveolar edema, capillary congestion, and neutrophilic infiltration, was observed in wildtype lungs and *Il2rg*$^{-/-}$*Rag2*$^{-/-}$ lungs reconstituted with wildtype NK cells. No acute histopathology was observed in sham lungs, and significantly attenuated injury was documented in *Il2rg*$^{-/-}$*Rag2*$^{-/-}$ lungs subjected to hilar clamp. Bars represent 100 μm. Injury metrics are shown in panels C through D with box and whisker plots illustrating individual data points, bound by boxes at 25th and 75th percentiles, and with medians depicted with bisecting lines. (C) Increased extravascular lung water was seen in hilar clamp wildtype lungs and hilar clamp *Il2rg*$^{-/-}$*Rag2*$^{-/-}$ lungs reconstituted with wildtype NK cells compared to both sham lungs and hilar clamp *Il2rg*$^{-/-}$*Rag2*$^{-/-}$ lungs. (D) Increased injury by gamma counts in dried lungs following systemic radiolabeled I^{125} albumin treatment were seen in hilar clamp wildtype lungs and hilar clamp *Il2rg*$^{-/-}$*Rag2*$^{-/-}$ lungs reconstituted with wildtype NK cells compared to both sham lungs and hilar clamp *Il2rg*$^{-/-}$*Rag2*$^{-/-}$ lungs. (E) Increased endothelial permeability was observed in hilar clamp wildtype lungs and hilar clamp *Il2rg*$^{-/-}$*Rag2*$^{-/-}$ lungs reconstituted with wildtype NK cells compared to sham lungs. All experiments studied 4–5 mice per condition. Differences were assessed by Kruskal_Wallis test (p values shown) and post-hoc comparisons with Dunn's test (brackets, *p<0.05, ** p<0.01, *** p<0.001). Data are reported from at least 3 independent experiments.

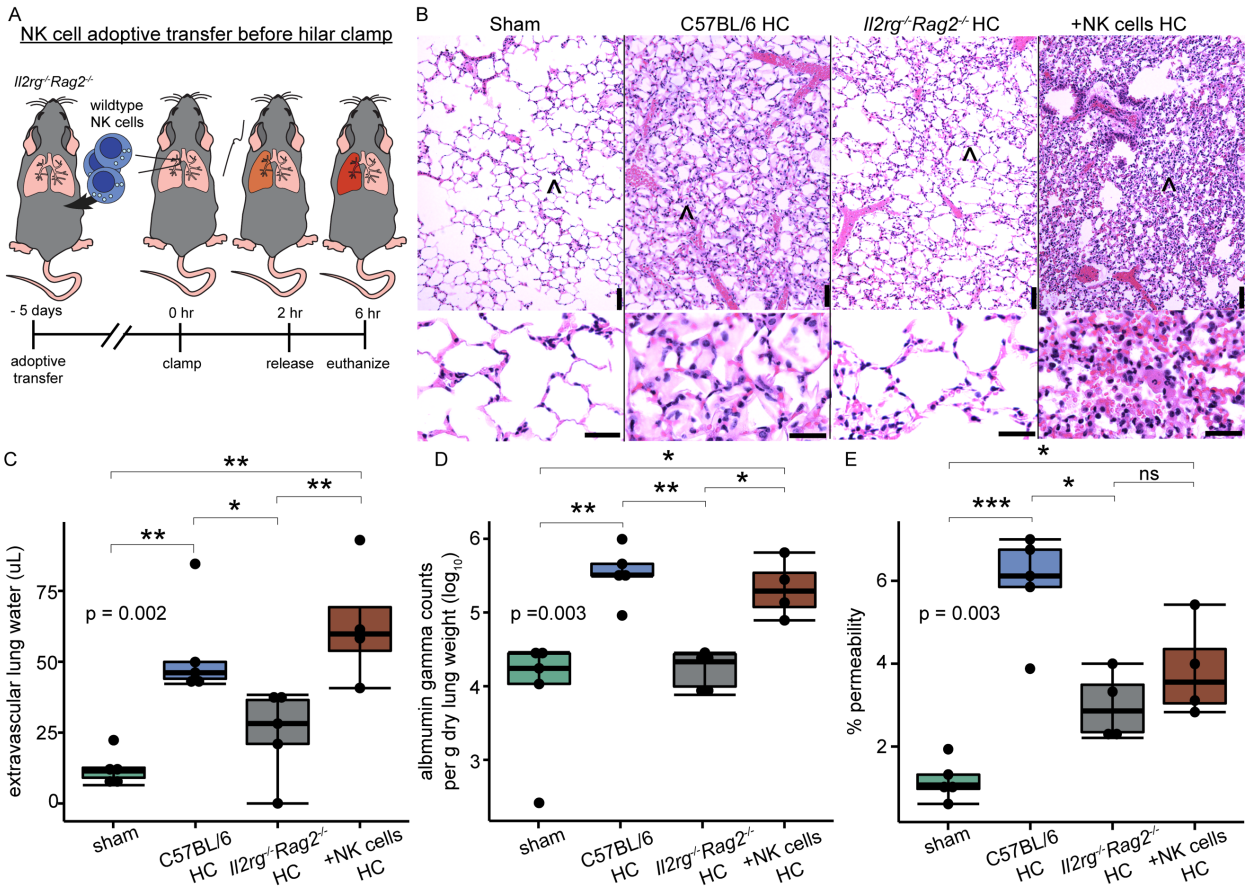
A
NK cell adoptive transfer before hilar clamp
Il2rg-/-Rag2-/-
wildtype NK cells
- 5 days
0 hr
2 hr
6 hr
adoptive transfer
clamp
release
euthanize
B
Sham
C57BL/6 HC
Il2rg-/-Rag2-/- HC
+NK cells HC
C
extravascular lung water (uL)
p = 0.002
sham
C57BL/6 HC
Il2rg-/-Rag2-/- HC
+NK cells HC
D
albumin gamma counts per g dry lung weight (log10)
p =0.003
E
% permeability
p = 0.003
ns

Figure 4. Mature NK cells are found in the lung tissue following experimental IRI. (A) To determine if NK cells were intravascular or in the tissue, PE-conjugated anti-NK1.1 mAb was injected intravenously following hilar clamp or sham procedures. In hilar clamp lungs, intravascular NK cells were decreased relative to sham lungs (B), and NK cells in the tissue increased (C). (D) Intravascular NK cells were mostly immature, but this population was decreased during hilar clamp. (E) In contrast, few tissue NK cells were immature. (F) Similarly, intravascular NK cells had a mature phenotype. (G) Following hilar clamp, the NK cells in the lung tissue were more mature than those in the sham lungs. Box and whisker plots show individual data points bound by boxes at 25^{th} and 75^{th} percentiles and medians depicted with bisecting lines. These experiments studied 4-5 mice per condition and differences were assessed with Mann-Whitney U test. (H) To visualize NK cell localization within lung tissue, we performed immunofluorescence. NK cells (NKp46, green) are seen in the extravascular space of bronchioles (nuclei highlighted by DAPI, blue) rather than within the vasculature (CD31, red) of mice undergoing hilar clamp compared to sham lungs.

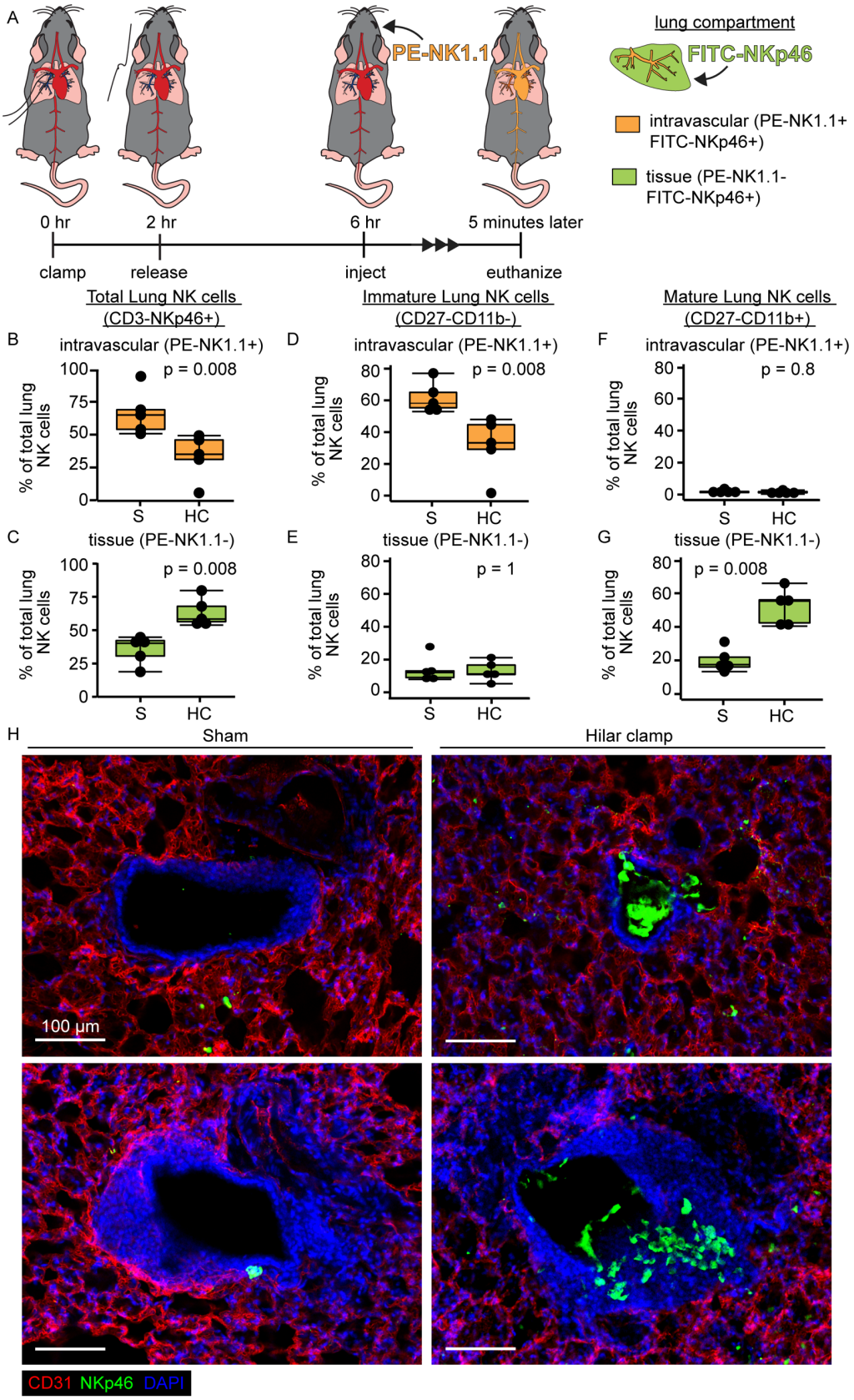
A
PE-NK1.1
lung compartment
FITC-NKp46
intravascular (PE-NK1.1+ FITC-NKp46+)
tissue (PE-NK1.1- FITC-NKp46+)
0 hr
2 hr
6 hr
5 minutes later
clamp
release
inject
euthanize
Total Lung NK cells (CD3-NKp46+)
Immature Lung NK cells (CD27-CD11b-)
Mature Lung NK cells (CD27-CD11b+)
B
intravascular (PE-NK1.1+)
p = 0.008
D
intravascular (PE-NK1.1+)
p = 0.008
F
intravascular (PE-NK1.1+)
p = 0.8
% of total lung NK cells
S
HC
C
tissue (PE-NK1.1-)
p = 0.008
E
tissue (PE-NK1.1-)
p = 1
G
tissue (PE-NK1.1-)
p = 0.008
H
Sham
Hilar clamp
100 µm
CD31 NKp46 DAPI

Figure 5. Lung NK cells exhibit a mature phenotype distinct from peripheral blood NK cells. To determine if NK cells expressed tissue-resident markers, lungs and peripheral blood were collected from C57BL/6 mice (n=4) following hilar clamp (n = 2) or sham (n = 2) procedures. Lung and blood NK cells were phenotypes by spectral flow cytometry and populations were identified based on expression of key markers. (A, B) Cell populations appeared to cluster by tissue origin, but not treatment condition. (C) L-selectin (CD62L) was decreased on lung NK cells relative to blood. Pulmonary NK cells displayed a more activated phenotype with increased CD16 (D), KLRG1 (E), Ly6c (F), and CD11b (G) and decreased CD27 (H) and DNAM1 (I). There were trends for decreased TRAIL (J) and NKG2A/C/E (K) in lung relative to blood NK cells. There was a positive correlation between KLRG1 and DNAM1 in the lung compared to the blood. Box and whisker plots show individual data points bound by boxes at 25^{th} and 75^{th} percentiles and medians depicted with bisecting lines. Differences were assessed with paired Student's t-tests (p) and statistically significant correlations ($p < 0.05$) between lung and blood NK cells are shown as Pearson's coefficient (r).

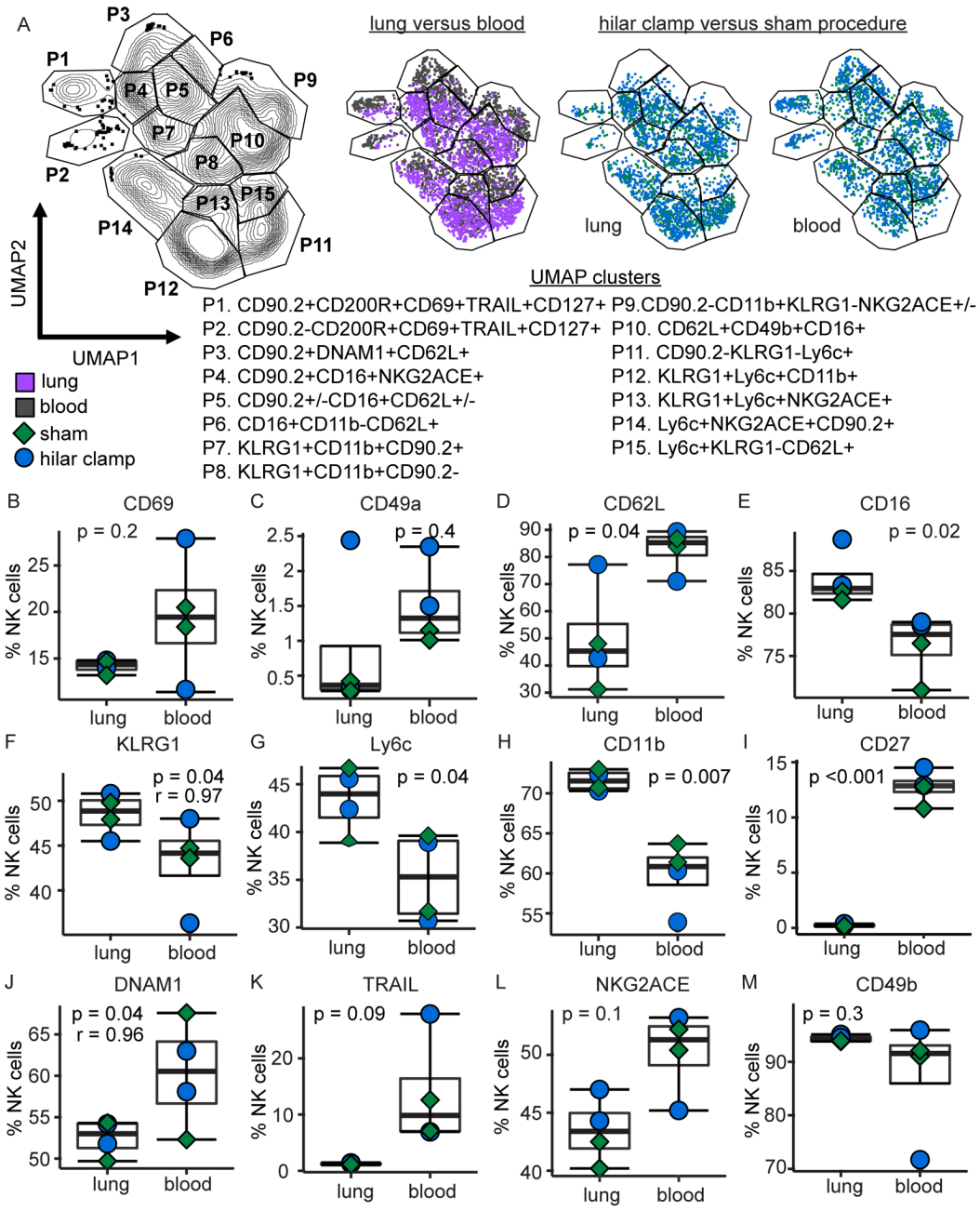
A
P3
P6
P1
P9
P4
P5
P7
P10
P8
P2
P13
P15
P14
P11
P12
UMAP2
UMAP1
lung
blood
sham
hilar clamp
lung versus blood
hilar clamp versus sham procedure
lung
blood
UMAP clusters
P1. CD90.2+CD200R+CD69+TRAIL+CD127+
P2. CD90.2-CD200R+CD69+TRAIL+CD127+
P3. CD90.2+DNAM1+CD62L+
P4. CD90.2+CD16+NKG2ACE+
P5. CD90.2+/-CD16+CD62L+/-
P6. CD16+CD11b-CD62L+
P7. KLRG1+CD11b+CD90.2+
P8. KLRG1+CD11b+CD90.2-
P9.CD90.2-CD11b+KLRG1-NKG2ACE+/-
P10. CD62L+CD49b+CD16+
P11. CD90.2-KLRG1-Ly6c+
P12. KLRG1+Ly6c+CD11b+
P13. KLRG1+Ly6c+NKG2ACE+
P14. Ly6c+NKG2ACE+CD90.2+
P15. Ly6c+KLRG1-CD62L+
B
CD69
p = 0.2
C
CD49a
p = 0.4
D
CD62L
p = 0.04
E
CD16
p = 0.02
F
KLRG1
p = 0.04
r = 0.97
G
Ly6c
p = 0.04
H
CD11b
p = 0.007
I
CD27
p <0.001
J
DNAM1
p = 0.04
r = 0.96
K
TRAIL
p = 0.09
L
NKG2ACE
p = 0.1
M
CD49b
p = 0.3
% NK cells
lung
blood

Figure 6. NK cells are increased and more mature in human allografts following PGD. (A) H&E and CD56 stains from representative surgical lung biopsies from 4 separate subjects at 3 (D3), 5 (D5), 20 (D20), and 30 (D30) days after lung transplantation. H&E preparations demonstrate PGD injury of diffuse alveolar septal thickening, edema, and type II pneumocyte hyperplasia. CD56+ cells are observed at sites of injury in each sample (bars 100 μm). (B) CD3+ cells were enumerated per high power field (HPF). (C) CD56+ cells were enumerated per HPF. (D) The median ratio of CD56+ cells to CD3+ cells in non-PGD allograft biopsy controls (n=6) was 0.3 IQR 0.22 – 0.39 and the median ratio of CD56+ cells to CD3+ cells in severe PGD (n = 7, p = 0.05) was 0.52 IQR 0.44 – 0.55. Differences between tissue immunohistochemistry cell counts were assessed with Student's t-test. (E) For the first 3 months following lung transplantation, bronchoalveolar lavage was prospectively collected during clinically indicated bronchoscopies. As a percentage of total lymphocytes, CD3-CD56+CD16+ NK cells were increased with severe PGD at post-operative day, considered as a binary outcome in generalized estimating equations-adjusted regression (p = 0.02). A similar increase in absolute numbers of CD16+ NK cells were increased with ordinal severity score for PGD (F, n = 94, p<0.001 by cumulative linked mixed model). (G) Ordinal PGD severity score also increased as a function of absolute numbers of CD16+ NK cells (p < 0.001 by cumulative linked mixed model). Box and whisker plots show individual data points bound by boxes at 25th and 75th percentiles and medians depicted with bisecting lines.

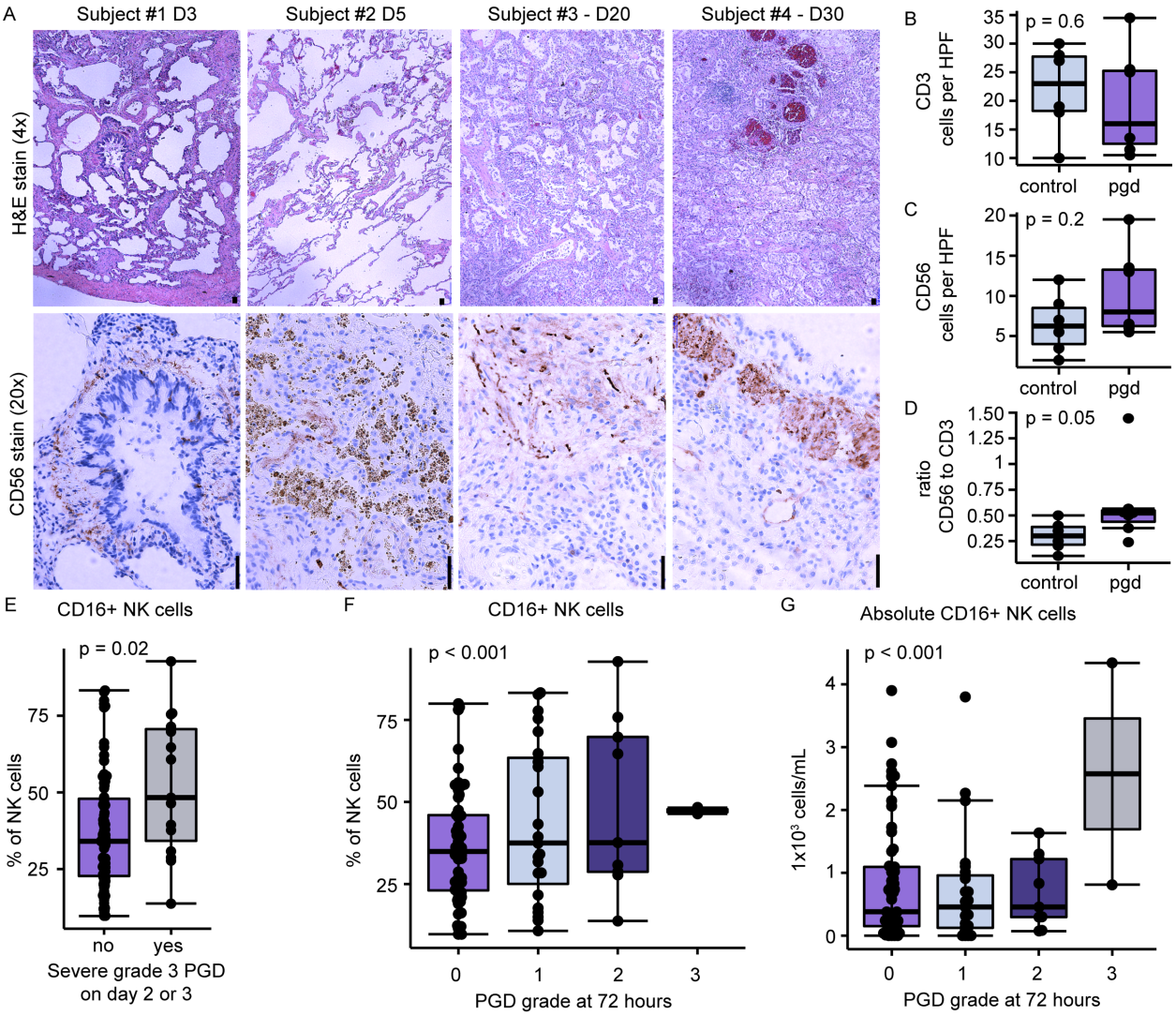
A
Subject #1 D3
Subject #2 D5
Subject #3 - D20
Subject #4 - D30
H&E stain (4x)
CD56 stain (20x)
B
CD3 cells per HPF
p = 0.6
control
pgd
C
CD56 cells per HPF
p = 0.2
control
pgd
D
ratio CD56 to CD3
p = 0.05
control
pgd
E
CD16+ NK cells
p = 0.02
% of NK cells
no
yes
Severe grade 3 PGD on day 2 or 3
F
CD16+ NK cells
p < 0.001
% of NK cells
PGD grade at 72 hours
G
Absolute CD16+ NK cells
p < 0.001
1x10³ cells/mL
PGD grade at 72 hours

Figure 7. NK cells are increased in a translational orthotopic lung transplant model with prolonged cold ischemia (OLT-PCI). (A) In the OLT-PCI model, donor lungs are harvested, stored for 18 hours at 4^{o}C, and transplanted for 8 hours of *in situ* warm reperfusion before mice are euthanized. (B) NK cells (CD3-NKp46+) were increased in dissociated lung tissue (HC) relative to sham procedures as a percentage of lymphocytes and (C) by total cell count. There were no differences in NKp46+ T cells (D, E), CD8+ T cells (F, G), or myeloid cells (H, I). (J) In the same OLT-PCI model, CD45.1 allotype donor lungs were transplanted into CD45.2 allotype recipient mice following prolonged cold ischemia. (K) Donor cells were identified by CD45.1 expression and recipient cells were identified as by CD45.2 surface expression. (L) Splenic lymphocytes were of recipient origin. (M) Over 80% of transplanted lung lymphocytes were also from the recipient. (N) 70% of the NK cells in the injured lung were of recipient origin. (O) The donor NK cells represented 30% of the donor lymphocytes, which was significantly more than the proportion of recipient NK cells. C57BL/6 donor and recipient mice were given depleting anti-NK1.1 or isotype-matched control monoclonal antibodies at 7 days and 24 hours preceding OLT-PCI. Differences were assessed using Student's t-test. Each condition studied at least 5 mice.

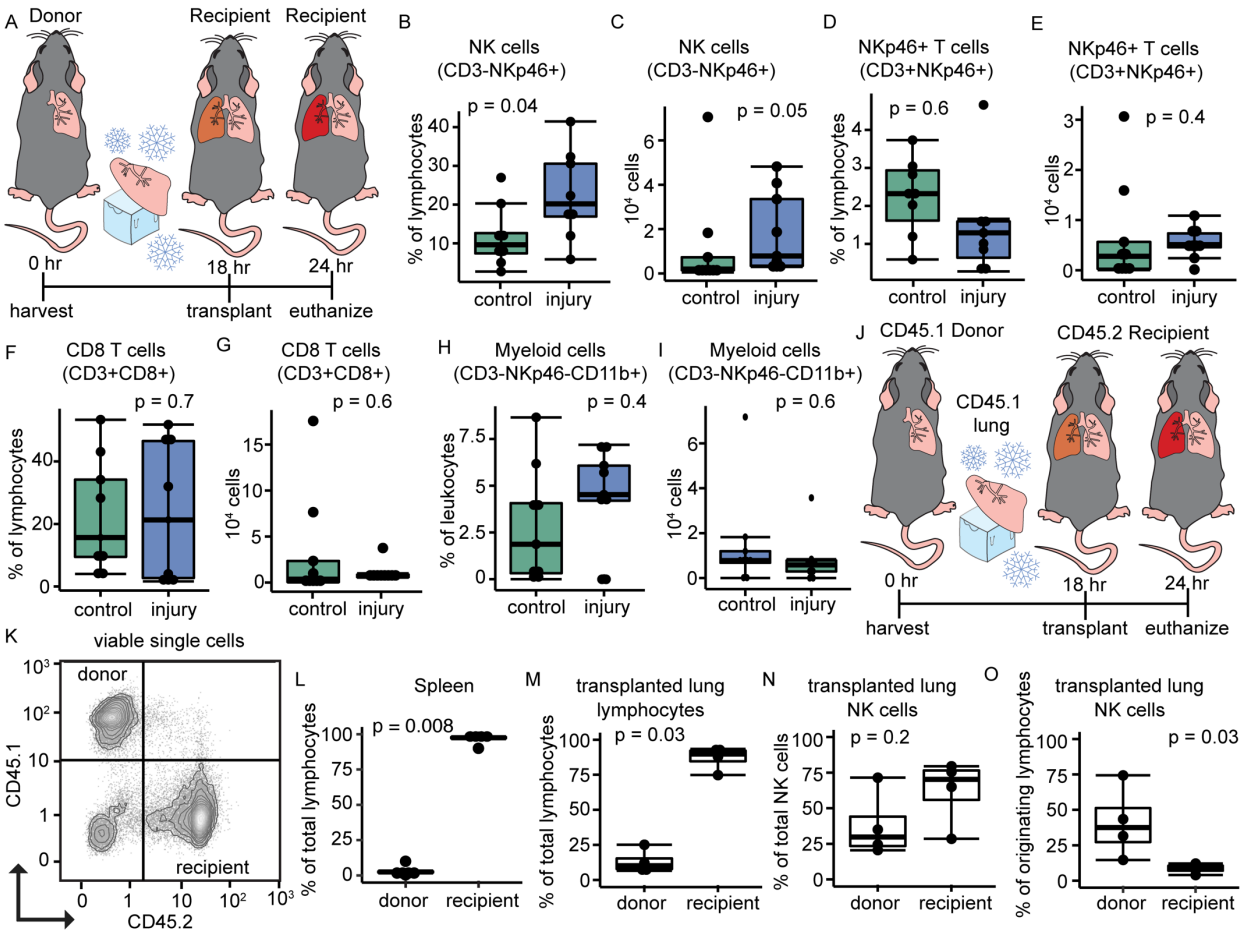
A
Donor
Recipient
Recipient
0 hr
18 hr
24 hr
harvest
transplant
euthanize
B
NK cells
(CD3-NKp46+)
p = 0.04
% of lymphocytes
control
injury
C
NK cells
(CD3-NKp46+)
p = 0.05
10⁴ cells
control
injury
D
NKp46+ T cells
(CD3+NKp46+)
p = 0.6
% of lymphocytes
control
injury
E
NKp46+ T cells
(CD3+NKp46+)
p = 0.4
10⁴ cells
control
injury
F
CD8 T cells
(CD3+CD8+)
p = 0.7
% of lymphocytes
control
injury
G
CD8 T cells
(CD3+CD8+)
p = 0.6
10⁴ cells
control
injury
H
Myeloid cells
(CD3-NKp46-CD11b+)
p = 0.4
% of leukocytes
control
injury
I
Myeloid cells
(CD3-NKp46-CD11b+)
p = 0.6
10⁴ cells
control
injury
J
CD45.1 Donor
CD45.2 Recipient
CD45.1
lung
0 hr
18 hr
24 hr
harvest
transplant
euthanize
K
viable single cells
donor
recipient
CD45.1
CD45.2
L
Spleen
p = 0.008
% of total lymphocytes
donor
recipient
M
transplanted lung
lymphocytes
p = 0.03
% of total lymphocytes
donor
recipient
N
transplanted lung
NK cells
p = 0.2
% of total NK cells
donor
recipient
O
transplanted lung
NK cells
p = 0.03
% of originating lymphocytes
donor
recipient

Figure 8. NK cells contribute to injury in a translational orthotopic lung transplant model with prolonged cold ischemia (OLT-PCI). (A) C57BL/6 mice were given anti-NK1.1 or isotype matched control antibody at 7 days and 1 day preceding OLT-PCI. (B) NK cells were successfully depleted from the lungs of animals receiving anti-NK1.1. Lung injury as measured by arterial PaO2 (C), left lung bronchoalveolar lavage protein (D), and left lung bronchoalveolar lavage neutrophil count (E) was significantly decreased in mice with NK cell depletion preceding OLT-PCI compared to isotype control mice. (F) H&E sections of e representative experiments are shown at 4x and 20x magnification from isotype and anti-NK1.1 lungs following OLT-PCI (bars 100 μm). Center for higher magnification from 4x images are denoted by "^." Differences were assessed using Student's t-test. Each condition studied at least 5 mice.

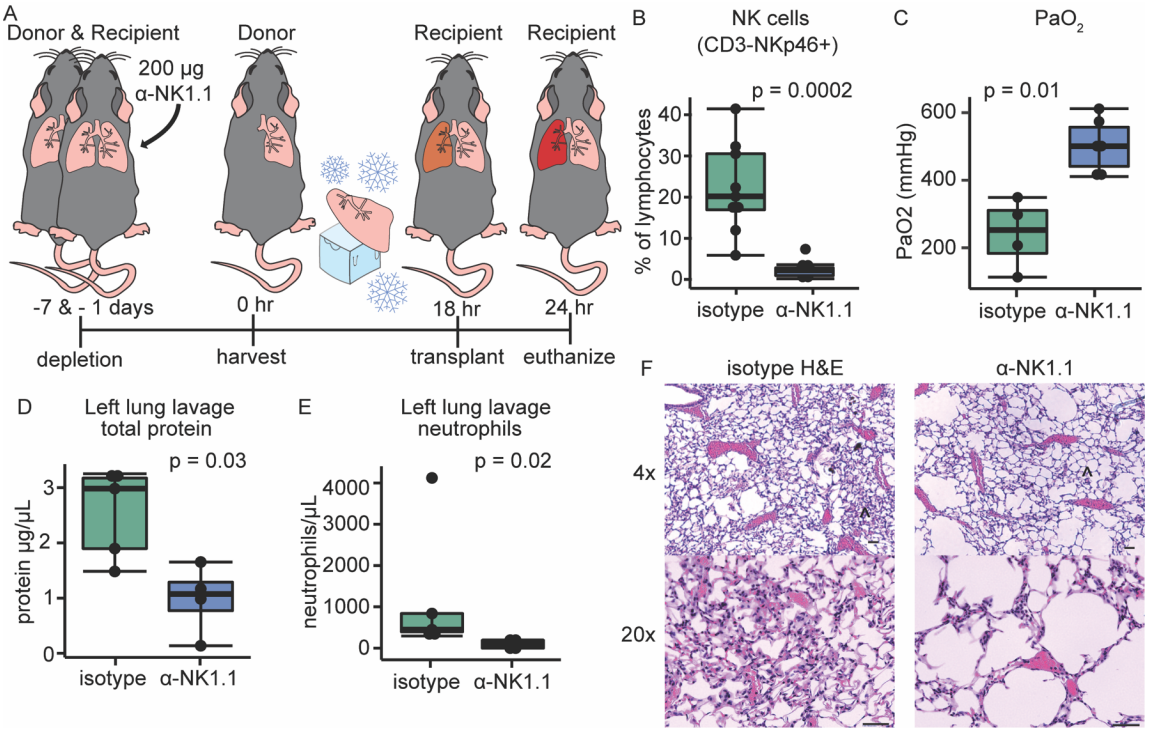

Figure 9. Recognition of stress molecules increased by IRI through the NKG2D receptor contributes to IRI pathology. (A) Following hilar clamp and sham procedures, epithelial cells (CD45-EpCAM+) and endothelial cells (CD45-PECAM-1+) were identified in dissociated lung. (B-E) Median fluorescent intensity and percentage of cells expressing MULT1 and RAE-1 were measured. MULT1 expression on epithelial cells was increased as a percentage (F) and by MFI (G) following hilar clamp. (H, I) The RAE-1 stress ligand was also increased on epithelial cells. (J, K) Endothelial MULT1 was not significantly different between hilar clamp and sham procedures. (L, M) Endothelial RAE-1 was increased following hilar clamp versus sham procedures. (N) Four conditions demonstrated the role of the NKG2D receptor in the hilar clamp model: (1) isotype control antibody or (2) NKG2D-blocking antibody was administered 7 days and 1 day preceding hilar clamp; (3) C57BL/6 NK cells or (4) NKG2D knock-out (*Klrk1*$^{-/-}$) NK cells were adoptively transferred into immunodeficient mice (*Il2rg*$^{-/-}$*Rag2*$^{-/-}$*).* Quantitative injury metrics were assessed for each condition and displayed as (O) extravascular lung water, (P) gamma counts of radiolabeled ^{125}I-albumin per gram of dry lung, and (Q) endothelial permeability. Box and whisker plots show individual data points bound by boxes at 25th and 75th percentiles and medians depicted with bisecting lines. Flow cytometry experiments studied 5 mice for each condition, antibody experiments studied 9-10 mice per condition, and adoptive transfer experiments studied 6-7 mice per condition. Comparisons between two groups were made with the Mann-Whitney U test, while group differences were assessed with the Kruskal-Wallis test using Dunn's test for post-hoc comparisons.

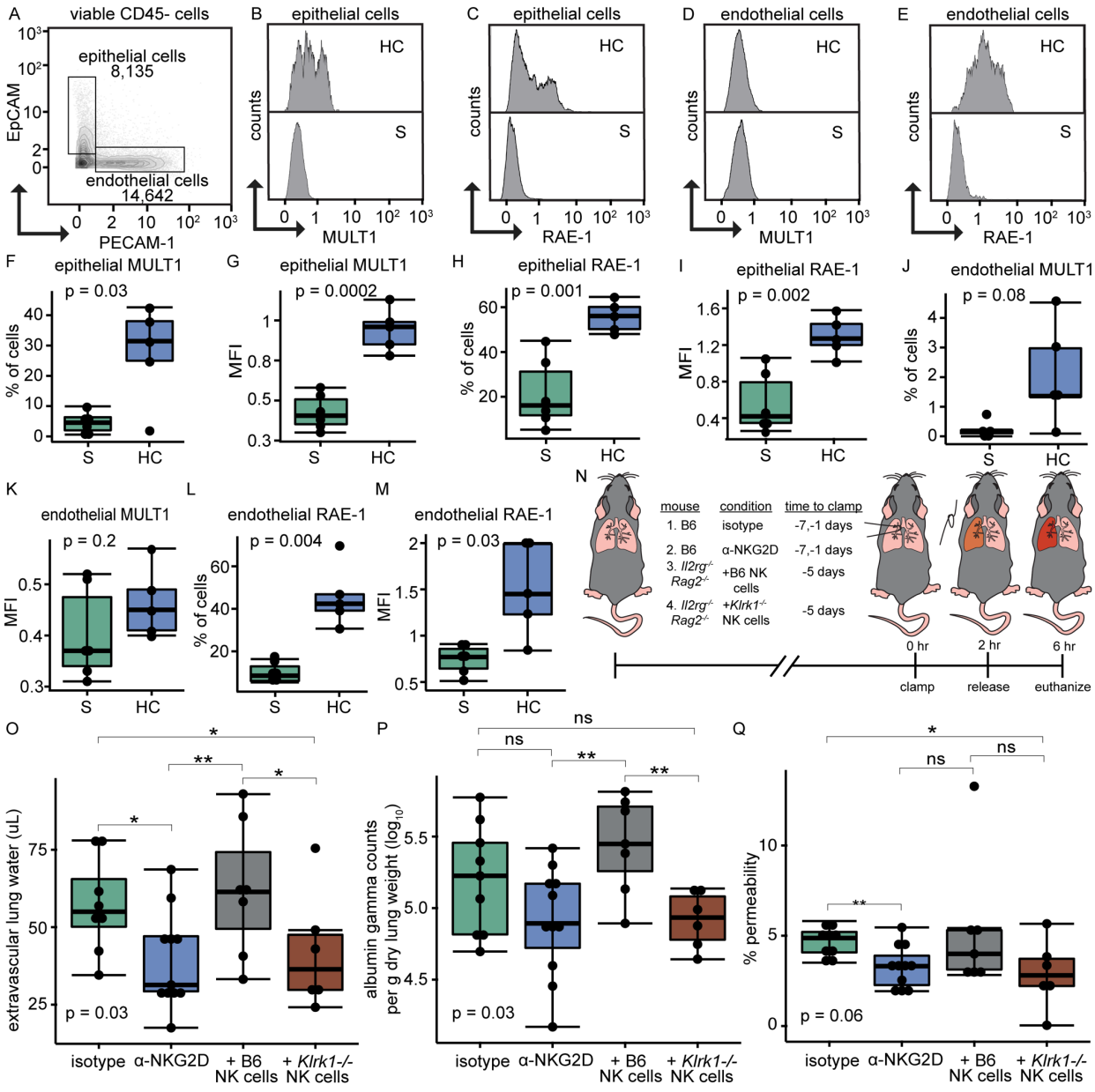
A
viable CD45- cells
epithelial cells
8,135
endothelial cells
14,642
EpCAM
PECAM-1
B
epithelial cells
HC
S
counts
MULT1
C
epithelial cells
RAE-1
D
endothelial cells
E
endothelial cells
F
epithelial MULT1
p = 0.03
% of cells
G
epithelial MULT1
p = 0.0002
MFI
H
epithelial RAE-1
p = 0.001
I
epithelial RAE-1
p = 0.002
J
endothelial MULT1
p = 0.08
K
endothelial MULT1
p = 0.2
L
endothelial RAE-1
p = 0.004
M
endothelial RAE-1
p = 0.03
N
mouse
condition
time to clamp
1. B6
isotype
-7,-1 days
2. B6
α-NKG2D
-7,-1 days
3. Il2rg-/- Rag2-/-
+B6 NK cells
-5 days
4. Il2rg-/- Rag2-/-
+Klrk1-/- NK cells
-5 days
0 hr
clamp
2 hr
release
6 hr
euthanize
O
extravascular lung water (uL)
p = 0.03
isotype
α-NKG2D
+ B6 NK cells
+ Klrk1-/- NK cells
P
albumin gamma counts per g dry lung weight (log10)
p = 0.03
Q
% permeability
p = 0.06